Diagnosing Inter-model variability of Northern Hemisphere Jet Stream Portrayal in 17 CMIP3 Global Climate Models

By

Sharon Clare Jaffe

A dissertation submitted in partial fulfillment of

the requirements for the degree of

Doctor of Philosophy

(Atmospheric and Oceanic Sciences)

at the

UNIVERSITY OF WISCONSIN-MADISON

2012

Date of the final oral examination: 5/16/2012

The dissertation is approved by the following members of the Final Oral Committee:

Jonathan E. Martin, Professor, Atmospheric and Oceanic Sciences

Daniel J. Vimont, Associate Professor, Atmospheric and Oceanic Sciences

Larissa E. Back, Assistant Professor, Atmospheric and Oceanic Sciences

Matthew H. Hitchman, Professor, Atmospheric and Oceanic Sciences

Samuel N. Stechmann, Assistant Professor, Mathematics

ACKNOWLEDGMENTS

The completion of my Ph.D. was made possible by the support of my colleagues, family, and friends. I am indebted to these people and consider our relationships to be more important than any possible academic achievement.

First, I thank my advisors: Dave Lorenz, Dan Vimont, and Jon Martin. Your diverse perspectives have been an exceptional source of ideas and have improved the quality of my research. I would like to thank Dave for his endless enthusiasm for jet stream dynamics as well as his patient explanations and confidence in my abilities. Dan contributed greatly to my project with his knowledge of how to creatively use statistics and his strong desire for me to gain scientific independence. I am so grateful for the encouragement, wise advice, and thoughtful teaching that I have received from my interactions with Jon.

I also thank my other scientific colleagues, including my committee members Larissa Back, Matt Hitchman, and Sam Stechmann as well as all the grad students with whom I have interacted during my time in Madison. My officemates, Andrea Lang, Andy Hulme, Brian Miretzky, Dan Hartung, Jace Bauer, Andrew Winters, and Pete Jzyk, have been great collaborators and friends over the years who have always been available to help brainstorm research ideas, discuss the weather, help with homework, and offer me encouragement.

I am also indebted to the AOS and CCR administrators, who make everything run so smoothly: Julie Niesen, Debbie Weber, Angel Skram, Toni Sumner-Beebe, Marrion Ladd, and many others. In addition, Pete Pokrandt and Kevin Braun were instrumental in the completion of my research as they continuously helped me solve computer and printer problems. I wish I could bring them both with me to my next job!

I thank the people of Zion Lutheran Church who have been my friends and role models over the past 5 years. They have continuously challenged me to grow and mature as we have journeyed together toward a fuller understanding of what is truly important in life.

Friends are the family that you choose for yourself and I have been lucky to have friends in Madison that have loved and supported me like family. They have spent countless hours brainstorming ideas with me, listening to my frustrations and stories, and are always there to celebrate when things go well. I truly thank Katie Holman, Erica Bickford, Val, Ninfa, and Lia Bennington, Morgan Maglio, and Sarah Davis for everything they have done and continue to do for me. I hope that wherever the future takes us we can remain like family.

I also thank my family, without whom this accomplishment certainly would not have been possible. Their constant and unconditional love gives me the strength to test myself without fear of failing. I thank my parents, Mary and Joel, my brother James, Grandma Gert, Grandma Joan, Grandpa Ed, Aunt Cheryl, Kari, and Erik (as well as my large and loving extended family). It is because of them that I am the person I am today.

Finally, I thank Sean. Being apart from you these last two years has been the hardest thing I have ever done. Thank you for your support of my education and career goals and your constant

love for me. Your commitment across the distance has been unwavering and I am so excited to start our life together.

This research was supported by NSF grant ATM-0653795, NOAA grant NA08OAR4310880, and NSF grant ATM-0806430. NCEP Reanalysis data was provided by the NOAA/OAR/ESRL PSD, Boulder, Colorado, USA, from their Web site at http://www.esrl.noaa.gov/psd/. In addition, we acknowledge the modeling groups, the Program for Climate Model Diagnosis and Intercomparison (PCMDI), and the WCRP's Working Group on Coupled Modelling (WGCM) for their roles in making available the WCRP CMIP3 multi-model dataset. Support of this dataset is provided by the Office of Science, U.S. Department of Energy.

TABLE OF CONTENTS

Page

LIST OF TABLES

LIST OF FIGURES

Figure Page

Appendix
Figure Page

Appendix
Figure Page

Appendix
Figure Page

ABSTRACT

The present study focuses on diagnosing inter-model variability of non-zonally averaged jet stream portrayal in 17 global climate models (GCMs) from the CMIP3 dataset. Knowledge of the factors underlying inter-model variability contributes to an improvement in the understanding of changes in jet stream structure due to anthropogenic climate change. Results presented here suggest that targeted improvement of simulated tropical Pacific sea surface temperatures (SSTs) will significantly improve the simulated extratropical circulation in models, of which the jet stream is a primary feature. In addition, reduced uncertainty in the ENSO response to global warming will lead to significant uncertainty reductions in the response of the jet as well.

This study begins with a historical overview of the Northern Hemisphere eddy-jet system. Next, the theorized effects of increased atmospheric carbon dioxide concentrations are introduced. The anthropogenic climate change impacts on the eddy-jet system include the direct response of an intensified mid-latitude jet stream and raised tropopause, and a secondary response of a poleward shifted jet. While both responses are evident in the ensemble mean 21st century projections, uncertainty in the poleward shift response is large enough that even the sign of the shift is not consistent among models, especially in the Northern Hemisphere.

The first part of the present analysis seeks relationships between mean winter 20th century model biases and (1) the internal modes of jet variability and (2) tropical SSTs. Compared to the reanalysis, the ensemble mean 300 hPa Atlantic jet is too zonally extended and located too far equatorward in GCMs. The Pacific jet varies significantly among modeling groups, with large biases in the vicinity of the jet exit region that cancel in the ensemble mean. Using maximum covariance analysis, it is found that 20th century Northern Hemisphere biases in upper-level winds are strongly related to an ENSO-like pattern in winter mean tropical Pacific SST biases.

Compared to the mean state, the temporal variability of the upper-level zonal winds in the 20th century is found to be accurately modeled in nearly all 17 GCMs. Also, it is shown that in the Pacific, model biases in the longitude of EOF 1 and 2 are strongly linked to the modeled longitude of the jet exit in the Pacific, indicating that the improved characterization of the mean state of the Pacific jet will positively impact the modeled variability.

The second part of the analysis finds that 21st century projections of the ensemble mean zonal wind change at 300 hPa predict a weakening and poleward expansion of the Pacific jet and an overall expansion of the Atlantic jet. These ensemble mean structures are somewhat different from the theorized poleward shift of the jet and do not consistently project onto model internal modes of variability. In contrast with the direct zonal mean climate change signal of increasing mid-latitude upper-level winds, 300 hPa zonal winds are projected to decrease in the core of the Pacific and Atlantic jets with increasing 300 hPa zonal winds located primarily in the jet exit regions and the meridional flanks of the jets.

Uncertainties in SST changes from the 20th to the 21st between models are shown to impact modeled Northern Hemisphere jet stream changes. In particular, ENSO-like mean winter SST changes explain 26% of inter-model variance of mid-latitude zonal wind compared to the 8% explained by the domain-averaged warming SST signal. This suggests that reduction of uncertainty in the ENSO response to global warming is very important because it will significantly reduce uncertainty in the Northern Hemisphere zonal wind response to climate change.

Chapter 1

Background

1.1 Eddy-Jet System: History, Dynamics, and Climatology

1.1.1 Jet Stream

As far back as the mid-19th century, in situ cloud observations and occasional balloon ascents engendered speculation regarding the existence of isolated high altitude wind speed maxima. However, the official "discovery" of the jet stream did not occur until 1944, during the final days of World War II (Reiter, 1963; Bryson, 1994). According to Bryson (1994), American bombers over Japan were hindered in their high-altitude missions because of the strong winds they encountered in the upper atmosphere, which were later termed "jet streams" by Carl Rossby (Reiter, 1963, 1967). Other accounts suggest that the German scientist Seilkopf introduced the name "Strahlströme" (jet stream) in 1939 (Reiter, 1963). These chance encounters with the jet stream advanced the field of meteorology, increasing the impetus for upper-level observations and more complete dynamical theories, and directly led to the early definition of the jet stream by the World Meteorological Organization: "A strong narrow current, concentrated along a quasi-horizontal axis in the upper troposphere or in the stratosphere, characterized by strong vertical and lateral wind shears and featuring one or more velocity maxima (Reiter, 1967).

Although the jet stream "surrounds the whole hemisphere in wavy meanders (Reiter, 1963), its two centers of maximum intensity in the Northern Hemisphere are located over the western Atlantic and western Pacific oceans, where hemispheric baroclinicity is maximized due to land-sea temperature contrast (Hoskins and Valdes, 1990). The Pacific jet is a well-defined maximum in zonal wind speed that extends from East Asia to the dateline in the Northern Hemisphere (NH). The region of mean acceleration of the zonal winds over East Asia is termed the jet entrance region and the region of mean deceleration of the zonal winds near the dateline is termed the jet exit region. The Atlantic jet tilts northeastward from the central continental United States toward Iceland and is less intense than the Pacific jet.

These Northern Hemisphere (NH) jets undergo a seasonal extension and intensification through early winter (November – January) as the NH mid-latitude baroclinicity increases, reaching their greatest zonal extent in February and then retracting and weakening through March and the early spring. The maximum intensity of the mean wintertime Pacific jet is located at approximately 33°N and 143°E, with a mean maximum wind speed of 57 m s^{-1} whereas the Atlantic jet maximum wind speed of 36 m s^{-1} occurs at 40°N and 70°W.

The intensity and position of the Northern Hemisphere jets fluctuate greatly on an intraseasonal basis, meaning that the winter climatology is not always characteristic of the state of the wintertime jet. Jet core wind speeds also fluctuate, with maximum wind speeds of 100 m s^{-1} or more present periodically throughout the winter. Common causes of intraseasonal variability of the Pacific jet include interactions with eddies composing the storm track and anomalies in tropical diabatic heating.

1.1.2 Storm Tracks

Cyclone tracks and their variability are intimately related to the jet mean state and variability. These connections are best approached through an understanding of the dynamics of storm tracks. Cyclonic storms are responsible for a great deal of the sensible weather that exists in the mid-latitudes. For this reason the lifecycle and track of mid-latitude storms have been studied for as long as meteorology has been considered a scientific endeavor. Early storm track research focused on identifying and classifying storms and their preferred tracks, leading to the publication of the first "global" (i.e. northern hemispheric) storm track maps in the Monthly Weather Review in 1872 (Klein, 1957). One seminal study by Klein (Petterssen, 1956; Klein, 1957), provided an early observational view of the two main Northern Hemispheric storm tracks: a Pacific cyclone track extending from the east coast of Japan toward the Gulf of Alaska and an Atlantic cyclone track from Alberta toward the upper Great Lakes and north Atlantic. Klein (1957) also identified two regions of maximum cyclone frequency: the Gulf of Alaska and the north Atlantic — coincident with the eastern flanks of the major storm tracks. His work was revolutionary because he observed that the position and intensity of storm tracks were related to the position and intensity of the 700 hPa wind speed maximum. His observations are consistent with our modern dynamical understanding of storm tracks and jet streams, but he made these assessments purely based on observations up to a pressure level of 700 hPa — a remarkable feat (Klein, 1957).

Storms tend to track from quasi-stationary troughs toward quasi-stationary ridges (where these troughs and ridges are part of the low-frequency circulation of the atmosphere) with maximum cyclone frequency located downstream and poleward of the climatological jet stream (Chang et al.,

2002). Storm tracks can be conceptualized as the preferred paths for cyclonic storms propagating eastward across the major ocean basins.

Storm tracks may be identified using a Lagrangian feature-tracking method or an Eulerian variance identification method. The feature-tracking method, which was predominantly used prior to the era of gridded data, identifies a storm/eddy based upon the location of a local sea level pressure (SLP) minimum as compared to a predetermined threshold value of SLP. Recently, storm tracks are more commonly identified using a maxima in the band-pass variance of geopotential height or wind (Sawyer, 1970; Blackmon, 1976; Blackmon et al., 1977). This Eulerian definition of a storm track is physically interpreted as a localized region in which increased SLP or geopotential height variability is present due to the frequent passage of SLP anomalies through that region (this definition does not distinguish between cyclones and anticyclones). For instance, the negative SLP anomaly due to the passage of a cyclone through a given region would lead to large SLP variability if that location was susceptible to the frequent cyclonic passage, as is the case in the storm track. Band-pass frequency filtering is typically used in order to focus on the characteristic 5–10 day life cycle of synoptic eddies.

The main mechanism responsible for eddy generation is baroclinic instability, which is maximized in the highly baroclinic region off the east coast of the Asian and North American continents, maintained by strong surface diabatic heating arising from the land-sea temperature contrast between the warm Kuroshio and Gulf Stream ocean currents and the extremely cold continental air to the west (Blackmon et al., 1984; Valdes and Hoskins, 1989; Orlanski, 1998). Baroclinic energy conversion is a central element in the energetics of mid-latitude weather disturbances in which the

mean flow potential energy stored in a meridional temperature gradient is transformed into kinetic energy of the transient waves, whose westerly tilt with altitude denotes their baroclinic nature (Charney, 1947; Eady, 1949). Eddy activity can be maintained by downstream development, in which individual synoptic eddies decay by transferring their energy to downstream eddies (Orlanski and Chang, 1993; Chang, 1993; Orlanski and Sheldon, 1995). The operation of downstream development means that baroclinic eddies develop not only from baroclinic energy conversion, but also from energy flux convergence originating in decaying disturbances located upstream (Orlanski and Sheldon, 1995). By its very nature, therefore, the process of downstream development actively extends the storm track (Orlanski and Chang, 1993; Simmons and Hoskins, 1979).

Despite these two vigorous eddy development mechanisms, the storm track is finite in zonal extent. Low-frequency disturbances (period $>$ 10 days) in the jet exit region decay through interactions with the mean flow by means of barotropic instability, in which kinetic energy of the eddies and the mean flow (jet) are exchanged and eddies lose (gain) kinetic energy through strengthening (weakening) the jet (Hoskins et al., 1983). In general, the baroclinic generation of energy drives the storm track, downstream development transports energy eastward from eddy to eddy, and eddy energy is dissipated through barotropic conversion enhanced in the diffluent jet exit region (Chang et al., 2002).

The relationship between the jet stream and the eddies/cyclones is complex and two perspectives are necessary in order to accurately portray the nature of this circulation system: that of eddies forcing the jet and that of the jet stream guiding the storm track. The jet stream (in addition to being forced by topography and diabatic heating) is internally forced by eddy heat and momentum

fluxes due to the transient eddies that compose the storm track (Lau, 1988). Also, the jet acts as a quasi-waveguide, trapping eddies in the jet core such that their meridional propagation is limited (Wallace et al., 1988). Furthermore, the variability in the jet stream and the variability of the eddies are related. Lorenz and Hartmann (2003) showed that eddy activity due to anomalies in the zonal wind field actually reinforces those zonal wind anomalies in the upper troposphere — a positive feedback.

One example of the complicated relationship between baroclinicity, cyclones, and jet streams is the mid-winter suppression of the Pacific storm track as originally defined by Nakamura (1992). It is unexpected that despite a maximum in baroclinicity over the Pacific basin during mid-winter months, storm track activity peaks in late fall and early spring and is at a minimum during the mid-winter months. Nakamura demonstrated that storm track activity varies with the speed of the Pacific jet stream, showing that the amplitude of baroclinic waves in the storm track increases as jet intensity increases only up to a jet speed of 45 m s^{-1}. Multiple theories have since been presented as to why this mid-winter suppression occurs, although the primary underlying mechanism for this suppression is still considered to be an open research question. A few of the suggested factors are 1) the jet stream is too strong during mid-winter months and waves quickly move through the baroclinicity without developing (Nakamura, 1992), 2) cyclone growth is deterred by a lack of moisture during mid-winter (Nakamura, 1992), 3) eddy seeds are blocked by the upstream Tibetan plateau during mid-winter because of the southward-shifted jet (Orlanski, 1998), or 4) the lowering of the tropopause acts to suppress the generation of eddy energy (Yin, 2002). Using theoretical models, Orlanski (2005) showed that the differences of wave seeds entering the storm track are a

main source of storm track variability (where a wave seed simply means an eddy from the Asian storm track that reaches the entrance to the Pacific storm track). As high-amplitude seeds flux energy downstream to upper-level waves, anticyclonic wave breaking may occur, which feeds back onto the large-scale stationary circulation by building up the ridge located in the eastern Pacific. In global climate model results, a decrease in eddy seeds entering the Atlantic storm track has been shown to lead to a decrease in Atlantic storm track activity during the last glacial maximum, despite an increase in baroclinicity (Donohoe and Battisti, 2009).

1.1.3 Tropical Heating Impacts

Many studies have documented the links between tropical diabatic heating anomalies (often identified as outgoing longwave radiation anomalies) and extratropical circulation anomalies. Hoskins and Karoly (1981) found that the thermal forcing due to a region of anomalous tropical convection causes strong upper-level divergence in the tropics and convergence in the subtropics, acting as a Rossby wave source. The consequent Rossby wave train develops and propagates out of the tropics following an approximate "great circle" route, with the disturbance moving to the north and east out of the tropics in the Northern Hemisphere. Through interactions with the mid-latitude storm track and zonally asymmetric circulation, a thermal forcing in the central tropical Pacific produces a disturbance that manifests itself as a series of height perturbations in the mid-latitudes that are equivalent barotropic in structure and spatially similar to the Pacific/North American (PNA) pattern (Wallace and Gutzler, 1981; Trenberth et al., 1998; Wang and Fu, 2000; Straus and Shukla, 2002). The PNA pattern is associated with the enhancement/extension and weakening/retraction of the Pacific jet (Wallace and Gutzler, 1981).

The extratropical response to a warm El Niño Southern Oscillation (ENSO) tropical heating anomaly looks similar to the positive PNA pattern (although not exactly alike), with enhanced subtropical Pacific westerlies and a strengthened and contracted Hadley Cell circulation (Trenberth et al., 1998; Wang and Fu, 2000; Lu et al., 2008; Straus and Shukla, 2002). ENSO influences may even be observed in the Atlantic region, although these effects are considerably weaker (Straus and Shukla, 2002). This means that tropical convection anomalies should be considered when examining potential influences on the structure of the Northern Hemisphere jets.

1.2 Climate Change and Jet Streams

Both an intensification and a poleward shift of the jet streams under anthropogenic climate change have been theorized (Chen and Held, 2007; Lorenz and DeWeaver, 2007; Kidston et al., 2011), observed over the past 30 years (Thompson and Wallace, 2000; Marshall, 2003; Hu et al., 2007; Johanson and Fu, 2009), and are broadly expected to continue into the future (Solomon, 2007), as shown in global climate models (GCMs). Understanding how the jet streams will change in the future is of primary importance in the assessment of anthropogenic climate change impacts. Jet streams are closely related to storm frequency and intensity across the mid-latitudes and a small change in jet position or intensity significantly impacts the sensible weather experienced by a large fraction of the populated world. Also, it is important that GCMs correctly model the large-scale circulation (of which the jet stream is a primary feature) in order to gain confidence in other variables that may be controlled by the large-scale circulation such as precipitation over North America related to the Pacific storm track.

1.2.1 Intensification of the Jet Stream

Increased atmospheric carbon dioxide concentrations cause the troposphere to warm and the stratosphere to cool. The troposphere warms because of increased absorption and re-emission of longwave radiation due to the greenhouse effect. The stratosphere cools as increased longwave emission to space outweights warming caused by the absorption of shortwave radiation by stratospheric ozone. The combined effect of tropospheric warming and stratospheric cooling decreases the static stability in the vicinity of the tropopause (as well as in the entire atmospheric column) and raises the height of the tropopause (Held, 1993; Lorenz and DeWeaver, 2007).

Also, despite the well-known surface polar amplification of the global warming temperature increase (Manabe and Stouffer, 1980; Serreze et al., 2009), the atmospheric column is warming more in the tropics than the poles (i.e. as measured by thickness increases), enhancing the pole-equator temperature gradient in the mid-latitudes. This is because air parcels in the tropics are constrained by radiative-convective equilibrium to follow a moist adiabatic lapse rate, leading to enhanced heating in the upper-tropospheric tropics compared to the mid-latitudes due to latent heat release (Held, 1993).

Both the downward slope of the tropopause from the equator to the poles and the thermal wind relationship dictate that a raised tropopause and enhanced pole-equator temperature gradient cause an intensification of the mid-latitude jet streams. Therefore, the direct effects of anthropogenic climate change include higher and more intense jet streams (Kushner et al., 2001; Lorenz and DeWeaver, 2007). In addition to the direct effects of climate change, a poleward shift of the jet streams has been simulated by climate models (Yin, 2005; Johanson and Fu, 2009; Lu et al., 2007;

Wu et al., 2010; Lorenz and DeWeaver, 2007; Kushner et al., 2001) and predicted statistically and dynamically.

1.2.2 Poleward Shift of Jet Stream: Statistical Physics Theory

The fluctuation-dissipation theorem (FDT) from statistical physics, first applied to climate science by Leith (1975), can be used to predict the climate response to small external forcings. FDT, suggests that a system's forced response will be related to the unforced internal modes of variability of the system (Leith, 1975). Therefore, FDT predicts that the forced response of mid-latitude winds to global warming will linearly project onto the internal modes of variability of unforced mid-latitude winds, assuming that climate perturbations are small enough for linear dynamics to hold (Ring and Plumb, 2008).

The northern/southern annular mode (NAM/SAM) structure (also called the Arctic/Antarctic Oscillation) is the dominant mode of hemispheric climate variability at all levels. NAM/SAM describes a north-south shift of mass between the mid-latitudes and the poles, indirectly describing a north-south shift of the polar (i.e. eddy-driven) jets (Thompson and Wallace, 2000). Based upon FDT, it has been hypothesized that the jet streams will shift meridionally under anthropogenic climate change as the forced climate change signal manifests as the amplification of NAM/SAM (Ring and Plumb, 2008; Gerber et al., 2008a). Studies have found that the time scale of the NAM/SAM is too long in GCM simulations (Gerber et al., 2008a), causing the extratropical jet to be too sensitive to global warming perturbations, validating the assumptions of FDT (Gerber et al., 2008b). It has also been shown that increased model resolution can improve the quality of

the modeled annular modes and improve the sensitivity of NAM/SAM to anthropogenic climate change (Gerber et al., 2008a).

In observations, the NAM and SAM have trended positive over the latter half of the 20th century, indicating a poleward shift of the polar jet in both hemispheres (Thompson et al., 2000; Marshall, 2003). However, the magnitude of this trend is currently in question because the annular mode structure has become significantly less positive since 2000 (Overland and Wang, 2005). Also, a recent study suggests that using the sea-level NAM/SAM, as is common practice, is ineffectual to describe jet shifts because it does not take into account the baroclinic structure of the anthropogenic climate change signal (Woollings, 2008).

Despite uncertainties, future projections of the NAM/SAM are certainly important. In fact, inter-model variance of the NAM in climate projections is shown to be responsible for up to 40% of surface temperature and precipitation variance over Eurasia and North America in late 21st century projections (Karpechko, 2010). A statistical physics perspective (FDT) suggests that the characterization of modeled internal variability is critical, even if the winter mean response to anthropogenic climate change is the main variable of interest (Gerber et al., 2008b). GCM portrayal of 20th century modes of internal variability of the jet will be examined in Chapter 2.

1.2.3 Poleward Shift of the Jet Stream: Dynamical Theory of the Eddy-driven Jet

A future poleward shift of the mid-latitude jet streams has also been explained dynamically by considering the interaction between changes in the zonal-mean jet and the eddies. One implication of the increased jet wind speeds due to the direct effects of climate change, described in 1.2.1, is

the increase of mid-latitude eddy phase speeds. Mid-latitude eddies are generated from baroclinic instability in the jet core. Later in the eddy life cycle they most often propagate equatorward (because of spherical geometry) and break before they reach the so-called "critical latitude" that restricts them, defined by the latitude at which the zonal wind equals the phase speed of the eddy. The faster the eddy phase speed, the less the waves deviate from the jet core throughout their life cycle (Chen et al., 2007). As eddy phase speeds increase, primarily in the jet core, as a direct result of global warming, the critical latitude moves poleward and eddies are confined closer to the jet core, shifting their associated eddy momentum fluxes produced during wave breaking poleward (Chen et al., 2007; Chen and Held, 2007). A poleward shift of eddy momentum flux divergence results in a poleward shift of tropospheric winds on the equatorward flank of the jet (Chen and Held, 2007; Chen et al., 2007; Lu et al., 2008).

Another dynamical mechanism that could be responsible for the poleward shift of the jets is the projected increase in spatial scale of mid-latitude eddies due to the decrease in overall static stability under global warming, as confirmed by GCM projections (Kidston et al., 2010). According to eddy dynamics, this increased spatial scale will cause a decrease in eddy phase speed with respect to mean tropospheric winds in the eddy source region at the jet core. Because slower eddies can travel farther before wave breaking occurs, these larger eddies will be more likely to propagate from the eddy source region before dissipating, increasing net wave propagation out of the source region (Kidston et al., 2011). Kidston et al. (2011) argue that this causes less eddy dissipation/wave breaking on the poleward side of the jet, making it more of a source region on average and suggesting a poleward expansion of the jet. Although it is possible that this mechanism will cause the

entire jet to shift polweward, it is also possible that it will result in a broader jet (Kidston et al., 2011).

A simpler mechanism proposes that because the tropical atmosphere is constrained to be moist adiabatic, tropospheric static stability will increase more on the equatorward flank of the jet than on the poleward flank, reducing baroclinicity on the equatorward flank of the jet. A decrease of baroclinicity decreases the number of waves generated in that region, decreasing the westerly forcing on the equatorward flank of the jet (Lu et al., 2010).

Despite the many mechanisms that could be responsible for shifting storm tracks poleward under anthropogenic climate change, interpreting future projections of storm track position is not straightforward. While some studies find that modeled storm tracks shift poleward by the end of the 21st century (Yin, 2005), other studies suggest a poleward expansion and intensification of future storm tracks (Wu et al., 2010). In general, the projected poleward shift of Southern Hemisphere (SH) storm tracks is much clearer and more robust than the shift of storm tracks in the Northern Hemisphere (NH), which is fraught with model discrepancies (Bengtsson et al., 2006; Ulbrich et al., 2008).

1.2.4 Poleward Shift of the Jet Stream: Dynamical Theory of the Subtropical Jet

Subtropical jet position may be inferred based upon the poleward extent of the Hadley Cell. The poleward boundaries of the Hadley Cell effectively represent the latitudinal extent of the tropical atmosphere and are coincident with the locations of the subtropical jets. The poleward boundaries of the Hadley cell are determined by the poleward extent to which angular momentum conservation

continues in the upper branch of the Hadley Cell. Lu et al. (2007) describe two main controls on the latitude at which angular momentum conservation breaks down: tropical tropopause height controlling tropical diabatic heating and static stability controlling the stability on the poleward flank of the subtropical jets (Lu et al., 2010).

Observational studies exploring a variety of reanalysis and OLR datasets show that a 2° – 4.5° latitude expansion of the Hadley Cell has occurred between 1979-2005 (Hu et al., 2007). While this time period may not be long enough to distinguish a long-term trend from decadal variability, this observed widening does not seem to be explained by internal atmospheric variability, which is less than 1.5° latitude in preindustrial GCM experiments (Johanson and Fu, 2009). GCMs project even more poleward expansion of the Hadley Cell in the future, averaging a 2° latitude expansion by the end of the 21st century (Lu et al., 2007). This estimate is much smaller than what has already been observed, supporting the assertion that the subtropical jet will translate poleward under anthropogenic climate change, perhaps more than estimates by GCMs suggest.

1.2.5 Poleward Shift of the Jet Stream: Zonal Winds in GCMs

Studies that have directly examined jet stream winds in global climate models (GCMs) have also lacked consensus with regard to modeled future jet stream structure, especially in the Northern Hemisphere. While the CMIP3 GCM ensemble mean zonal mean zonal winds show a poleward shift and intensification of the jet (Lorenz and DeWeaver, 2007; Kushner et al., 2001), the inter-model spread is larger than the ensemble mean, reducing confidence in GCM projections (Kidston and Gerber, 2010; Woollings and Blackburn, 2012). Overall, a poleward shift of low-level winds (such as 850 mb or surface) is more consistent between modeling groups, perhaps indicating that

the polar eddy-driven jet, which penetrates into the lower troposphere, unlike the subtropical jet, has a clearer response to anthropogenic climate change (Woollings and Blackburn, 2012).

Because of the possible differences between subtropical and polar jet responses to anthropogenic climate change, studies that do not use a zonal mean perspective have found distinct results for different local jet stream structures. For instance, one recent observational study has shown that the NH Atlantic jet has shifted northward while the NH Pacific (East Asian) jet has not (Yaocun and Daqing, 2011). Intensification of upper-level wind has been shown to be consistent among GCMs, while the possible projected poleward shift of jet stream winds in the NH Atlantic and Pacific regions varies widely among modeling groups (Ihara and Kushnir, 2009).

Adding complexity to the situation, all CMIP3 GCMs have been found to position the zonal mean jet too far equatorward in both hemispheres in the 20th century when compared to reanalysis data (Kidston and Gerber, 2010; Woollings and Blackburn, 2012). Because 21st century projections of jet structure are correlated with 20th century jet model biases (Kidston and Gerber, 2010), an important step toward understanding future jet stream structure is a careful analysis of 20th century model biases.

1.3 Outline

Future changes in the jet stream are not robust in CMIP3 GCMs, especially in the Northern Hemisphere (Lorenz and DeWeaver, 2007; Kushner et al., 2001; Kidston and Gerber, 2010; Woollings and Blackburn, 2012; Yaocun and Daqing, 2011; Ihara and Kushnir, 2009). The present

study focuses on understanding reasons for inter-model variability of non-zonally averaged zonal wind in both the 20th century and the 21st century response to climate change.

Chapter 2 examines the 20th century mean winter model bias, seeking relationships between model bias, internal modes of jet variability, and tropical SSTs. The robustness of jet variability in GCMs is also examined in Chapter 2. Chapter 3 analyzes 21st century projections of jet stream structure in order to diagnose what underlies inter-model variations in jet stream change. The role of internal modes of variability and tropical Pacific SSTs are examined using maximum covariance analysis (MCA) and regression analysis. Final conclusions and future avenues of research are discussed in Chapter 4.

Chapter 2

20th Century Jet Stream Biases in GCMs

2.1 Background

A poleward shift of the jet streams under anthropogenic climate change has been theorized (Chen and Held, 2007; Lorenz and DeWeaver, 2007; Kidston et al., 2011), observed over the past 30 years (Thompson and Wallace, 2000; Marshall, 2003; Hu et al., 2007; Johanson and Fu, 2009), and is broadly expected to continue into the future (Solomon, 2007). Despite the multitude of studies acknowledging this poleward shift, jet stream winds still vary significantly between observational datasets and modeling groups.

Because 21st century projections of jet structure are correlated with 20th century jet model biases (Kidston and Gerber, 2010), the next step toward understanding future jet stream structure is a careful analysis of 20th century model biases, as presented here. The goal of Chapter 2 is to understand why there is a lack of model consensus of NH jet structure in 20th century simulations. Chapter 3 will then discuss how to use this knowledge of 20th century simulations to better understand 21st century projections. While analyses of the zonal mean wind are a good starting point for an examination of the large-scale circulation, this study goes one step further to look at the upper-level winds separately for the Atlantic and Pacific basins without the use of zonal averaging. This

type of analysis is valuable because of the complex jet dynamics associated with the asymmetric NH circulation.

Chapter 2 is organized as follows. Section 2.2 outlines the reanalysis and GCM data used in this study. Results of a detailed comparison between GCM simulations and reanalysis are presented in Section 2.3. These results include the analysis of ensemble mean winter biases as well as an examination of inter-model variations and the portrayal of jet stream variability in GCMs. The main analysis tools used are empirical orthogonal function/principal component (EOF/PC) analysis and maximum covariance analysis (MCA). Conclusions for Chapter 2 are found in Section 2.4.

2.2 Data and Methods

In this study, observations are used to establish a climatology of NH jet streams based upon the 1980-1999 mean winter zonal winds. These observations come from the NCEP/NCAR Reanalysis1 dataset (Kalnay et al., 1996). Seventeen GCMs are assessed in comparison with the observations to determine the accuracy of jet stream characterization in each model. These 17 GCMs come from the World Climate Research Programme's (WCRP's) Coupled Model Intercomparison Project phase 3 (CMIP3) multi-model dataset for the climate of the 20th century experiment (20c3m) [1]. Table 2.1 lists the models included in this study. These particular models are chosen because they provide the daily-resolved data required for this study.

The present study employs daily 300 hPa zonal wind data and monthly sea surface temperature (SST) data for 20 boreal winter seasons. A complementary analysis using 700 hPa zonal wind data (not discussed) is found to be in close agreement with the results at 300 hPa. Daily wind data are

[1] http://www-pcmdi.llnl.gov/ipcc/model_documentation/ipcc_model_documentation.php

smoothed using a 5 day running mean for the period encompassing November 1 through March 31st of each winter from November 1979 to March 1999 (with leap days removed). The 17 GCMs vary in resolution from 1.125° latitude x 1.125° longitude (Model 1 - INGV-SXG) to 4° latitude x 5° longitude (Model 17 - INM-CM3.0). In order to directly compare model and reanalysis data, each model is linearly interpolated to 2.5° latitude x 2.5° longitude resolution. Resolution differences between models are not found to be related to the accuracy of jet stream portrayal.

To create the mean winter zonal wind (SST), the smoothed (monthly) data are averaged over NDJFM and over all 20 years of the data period. The seasonal cycle of zonal wind is created by averaging each smoothed day (i.e. pentad) over all 20 boreal winter seasons. Smoothed daily wind data (with the seasonal cycle removed) are used to perform EOF/PC analysis.

2.3 Results and Discussion

2.3.1 Jet portrayal in NCEP/NCAR reanalysis

Both the mean state and variability of the upper-level winds are examined in order to gain a full understanding of the NH jet streams in reanalysis data, which is then used to assess GCM accuracy. The reanalysis winter mean 300 hPa zonal wind for 1980-99 is shown in Figure 2.1, with wind speed maxima located in the Pacific and Atlantic basins (hereafter called the Pacific and Atlantic jets). The Pacific jet extends from East Asia across the Pacific basin and the Atlantic jet extends from the central continental United States to the west coast of Europe, tilting northeastward across the Atlantic basin.

The dominant modes of variability of the reanalysis are identified through empirical orthogonal function/principal component (EOF/PC) analysis of the smoothed daily 300 hPa zonal wind field

with the seasonal cycle removed. EOF/PC analysis is performed on the reanalysis data over the North Atlantic (120°W - 20°E, 22.5°N - 80°N) and the North Pacific (100°E - 240°E, 22.5°N - 80°N) basins for winter (NDJFM) 1980-99. All EOFs/PCs shown in this study have been found to be well separated from higher-order EOFs/PCs as determined by the methodology of North et al. (1982). The two dominant modes of variability for each basin are shown in Fig. 2.2 as regressions of the 300 hPa zonal wind field (0° - 80°N) onto the first and second PCs of the zonal wind. These dominant modes of variability represent the most likely ways the jet stream will vary from its average position.

In the Pacific, the primary mode of variability explains 15.9% of the variance in the upper-level zonal wind, with the dominant variant structure located near the jet exit region (Fig. 2.2a), indicating a strengthening and weakening of zonal winds in this region. This mode represents an extension or retraction of the upper-level jet (Jaffe et al., 2011). The secondary mode of variability in the Pacific explains 11% of the variance in the upper-level zonal wind and looks quite different from the primary mode of variability, with a dipole of variant structures straddling the jet axis near the jet exit region (Fig. 2.2b). This pattern represents a northward/southward shift of the jet near the exit region.

In the Atlantic the first mode of variability (21% of the total variance) resembles a northward/southward shift of the eastern half of the jet (Fig. 2.2c) and the second mode of variability (18% of the total variance) characterizes a strengthening/weakening of the zonal wind speed in the jet core especially in the eastern half of the jet (Fig. 2.2d). Because the structure of the Atlantic jet includes a southeast-northwest oriented tilt from southeastern North America toward

Great Britain, an additional level of complexity is added to the interpretation of these patterns of variability. To be certain of the correct interpretation, a composite analysis is performed, averaging over the smoothed daily data that have PCs 1-2 greater than 1 standard deviation (or less than -1 standard deviation). This threshold includes the pentads with the largest magnitude variability of the upper-level winds. Results are shown in Fig. 2.3 with the perturbation winds associated with each composite in the left panel and the full winds in the right panel for each case. The composite analysis supports the interpretation that the primary mode of variability of the Atlantic jet is a more like a northward/southward shift and the secondary mode of variability is more like a strengthening/weakening of the jet exit region. The northward/southward shift of the jet can be seen by comparing Fig. 2.3b and Fig. 2.3d and the extension/retraction of the jet can be seen by comparing Fig. 2.3f and Fig. 2.3h The composite retraction of the Atlantic jet (Fig. 2.3h) also strongly resembles a blocking pattern over the Atlantic basin.

Although the two leading modes of variability in the Pacific and Atlantic basin are opposite one another, they can be interpreted similarly. To add meaning to the discussion of these modes of variability they will be referred to as the "Shift EOF" (Pacific EOF 2 and Atlantic EOF 1) and "Extend/Retract EOF" (Pacific EOF 1 and Atlantic EOF 2) throughout the remainder of the study. It has been suggested that the reversal of the primary and secondary modes of variability between the Pacific and Atlantic jets results from differences in the orientation of the subtropical and eddy-driven jets in the two regions (Eichelberger and Hartmann, 2007). This is likely related to the distinct nature of the jet in each region, with the upper-level winds in the Pacific dominated by the influence of the subtropical jet stream, and the upper-level winds in the Atlantic influenced by both

the polar and subtropical jet streams (Lorenz and Hartmann, 2003; Eichelberger and Hartmann, 2007). The difference between these two regions is important and would not be apparent in a zonal mean analysis of the NH jets.

2.3.2 GCM bias of the mean winter jet

Model bias is defined to be the difference between the GCM and reanalysis 300 hPa zonal wind ($U_{bias} = U_{GCM} - U_{reanalysis}$). A positive model bias indicates that modeled westerly zonal wind speeds are too high in a given location and negative model bias shows where modeled zonal wind speeds are too low. Figure 2.4a shows the average model bias for the 17 GCMs being considered. Overall, model bias of the upper-level zonal wind is on the same order of magnitude as the two dominant modes of variability seen in Fig. 2.2. Also, the amplitude of the average model bias is of the same order of magnitude as the standard deviation of model bias around the ensemble mean (Fig. 2.4b).

The largest bias of the model mean occurs in the Atlantic, where the jet is too extended and positioned too far equatorward on average in the models. The modeled jet is also positioned too far equatorward in the Southern Hemisphere (not shown), supporting the results of Kidston and Gerber (2010). The bias of the model mean in the Atlantic is somewhat larger than the standard deviation about the ensemble mean, indicating that biases are fairly consistent across models in this basin. The standard deviation for the Atlantic jet is positioned farther west than the mean model bias, with two maxima located on the poleward and equatorward flanks of the Atlantic jet.

Compared to the Atlantic, the bias of the model mean is small in the Pacific, with one isolated region of positive bias in the Eastern Pacific and another weak region of positive bias on the

poleward flank of the Pacific jet. However, the standard deviation of models about the ensemble mean is quite large, indicating that models exhibit much variability in their portrayal of the Pacific jet. The standard deviation is largest, more than 8 m s^{-1}, in the Pacific jet exit region, strongly resembling the dominant mode of variability (EOF 1 - Extension/Retraction) for the Pacific region.

An examination of individual model portrayals of the mean winter jets (representative examples shown in Fig. 2.5) shows that some models have very small biases (Figs. 2.5a and 2.5b) while other models have bias patterns that resemble the dominant modes of variability of the observed winter jet (Figs. 2.5c to 2.5f).

As a first step toward understanding the cause of model biases, it is important to determine the relationship of these biases with the dominant modes of variability in the Pacific and Atlantic regions. Such relationships offer clues regarding the existence of model biases. A normalized projection of each model's mean winter bias onto the first and second EOFs of the upper-level zonal wind from the reanalysis (shown in Fig. 2.2) is used to quantify the relationship between the model biases and the observed modes of jet variability. This analysis is done separately for the Atlantic (120°W - 20°E) and Pacific (100°E - 120°W) basins and results are shown in Fig. 2.6. The sign convention used for the EOF 1-2 patterns of the reanalysis is that shown in Fig. 2.2. The position of each point with respect to the x-axis (y-axis) shows the value of each model's projection onto EOF 1 (2) from the reanalysis.

In the Pacific, the projection of each model's bias onto the observed dominant modes of variability shows two clusters of models. The first group of models (Group 1, depicted with crosses) have biases clustered on the negative x-axis, indicating their similarity to a retraction of the Pacific

jet (negative EOF 1). The second group of models (Group 2, depicted with asterisks) have biases clustered on the positive x-axis, indicating their similarity to an extension of the Pacific jet (positive EOF 1). These two groups of models also have different positions with respect to the y-axis, with Group 1 being more likely to have a bias resembling a northward shift of the Pacific jet (positive EOF 2) and Group 2 being more likely to have a bias resembling a southward shift of the Pacific jet (negative EOF 2). It is important to note that while these two groups are well-separated in EOF space, the length of their projections onto EOF 1-2 are only $\sim$0.5-0.6, indicating that EOF 1-2 are not complete in their explanation of bias in this case. The black line connects the average Group 1 projection to the average Group 2 projection, showing the axis along which a combination of EOF 1 and 2 explain the inter-model bias of the upper-level zonal wind. The segregation of models along this axis is unusual and merits further examination. The open circles and diamonds in Fig. 2.6 will be explained in relation to other results discussed in section 2.3.3.

In the Atlantic (Fig. 2.6b), models biases are more uniform, without the distinctive two group structure found for the Pacific. Atlantic model biases mostly cluster in quadrant 4, resembling both an extension and southward shift of the Atlantic jet (negative EOF 1 and positive EOF 2). In Fig. 2.6b Atlantic models continue to be depicted as crosses/asterisks according to their respective groups as determined for the Pacific — and a delineation is still apparent between Group 1 and Group 2. This delineation is shown by the fact that crosses and asterisks barely overlap despite the fact that they are all located in the vicinity of quadrant 4 in Fig. 2.6b. The fact that this grouped bias structure holds true in the Atlantic suggests that despite the differences between the two basins, model biases in the Atlantic and Pacific regions are likely linked.

In order to uncover the difference in spatial structure between Group 1 and Group 2, the mean model bias of each group is calculated. The difference between Group 1 and Group 2 ($Group\ 2 - Group\ 1$) is shown in Fig. 2.7. There are two maxima, which indicate regions of oppositely-signed bias between Group 1 and 2. The first (and largest) maximum in bias difference is found in the Pacific jet exit region, in the same location as the large value of the standard deviation of model bias shown in Fig. 2.4b. The second maximum in bias difference is found on the southern flank of the Atlantic jet, also found in a location of high standard deviation of model bias, as shown in Fig. 2.4b. No significant difference between Group 1 and Group 2 is found in the Southern Hemisphere (not shown).

2.3.3 Relationship between jet bias and tropical Pacific SST bias in GCMs

The strong link between biases in the Pacific and Atlantic basins (despite different jet dynamics in each region) suggests that a forcing external to the mid-latitude eddy/jet system is involved in producing these model biases. Due to the far reaching influence of El Niño Southern Oscillation (ENSO), this system will be considered as a possible external forcing influencing model biases of mid-latitude upper-level winds. This potential relationship will be examined using maximum covariance analysis (MCA).

MCA is used here to assess the dominant patterns of covariability between tropical SST biases and upper-level zonal wind biases in the same models. This technique identifies pairs of patterns that maximize the squared covariance between two variables: in this case the mid-latitude 300 hPa zonal wind (100°E - 20°W, 10°N - 80°N) and the tropical SST (30°S - 30°N, 120°E - 290°E). The covariance is identified across a given sampling dimension. Typically sampling is performed

across time, but in this case sampling is done across the 17 GCMs to identify structures linked to model bias. Further explanation of MCA may be found in Bretherton et al. (1992), Wallace et al. (1992), and Deser and Timlin (1997). It is important to note that because this MCA analysis samples across model space instead of across time, ENSO-like SST patterns that are identified are not equivalent to inter-annual variability in any model. Instead, these ENSO-like patterns of SST show the winter mean state of the tropical Pacific that is associated with a given mode of inter-model covariability.

The first mode of covariability between the wind and SST explains 52% of the total squared covariance between the two fields. Considering that the second and third modes of covariability explain 16% and 13% of the total covariance respectively, the first mode is clearly dominant. Confirming the validity of this technique, the normalized root mean squared covariance (NRMSC) is calculated to be 0.30, meaning that there is a significant amount of total covariance between these two fields. In addition, the correlation between the two expansion coefficients (i.e. the left and right singular vectors) is 0.81, verifying that there is a high degree of coupling between the patterns identified in the wind and SST fields (Fig. 2.8c). Therefore, the first pattern of covariability identified by MCA appears robust and is shown in Fig. 2.8.

The patterns of covariability produced by MCA are depicted via regressing SST bias (homogeneous; Fig. 2.8b) and zonal wind bias (heterogeneous; Fig. 2.8a) onto the SST expansion coefficient. Regression onto the zonal wind expansion coefficient yields similar structures. Here we focus on the SST expansion coefficient as a potential predictor of zonal wind bias. A scatter

plot of the SST and zonal wind expansion coefficients is depicted in Fig. 2.8c, and demonstrates their strong correlation.

The homogeneous SST field (Fig. 2.8b) strongly resembles the positive phase of ENSO and exhibits a high spatial correlation with the observed ENSO SST pattern, shown in Fig. 2.9b (r = 0.70), with further discussion to follow. The heterogeneous wind field (Fig. 2.8a) is similarly spatially correlated with the grouped model bias shown in Fig. 2.7 (r = 0.81). It is notable that ENSO-like SST biases are so directly connected to mid-latitude jet biases through the first mode of covariability produced by MCA. This indicates that the portrayal of the winter mean state in the tropical Pacific affects the modeled upper-level midlatitude zonal winds in both the Pacific and Atlantic regions, suggesting that differences in NH jet stream portrayal between the 17 GCMs are primarily related to the representation of ENSO-like mean SST in the tropical Pacific.

The open circles added to Fig. 2.6 seek to explain the relationship between the grouped model bias and the ENSO-like structure of tropical Pacific SST biases. The open circles show the values of the normalized projection of the heterogeneous wind pattern (Fig. 2.8a) onto the primary and secondary modes of zonal wind variability from the reanalysis data (EOF 1-2, Figs. 2.2a to 2.2d) for the Pacific (2.6a) and Atlantic (2.6b) regions. Because of the non-signed nature of MCA, the open circles show both possible sign conventions. The addition of these circles show that the portion of the model wind bias due to ENSO-like mean SST biases in the tropical Pacific falls along almost the same axis as the bias of the jet stream between models in the Pacific (2.6a). This reinforces the hypothesis that the uncertainties in mean winter Pacific jet stream portrayal are caused by each model's treatment of winter mean tropical Pacific SST and suggests that if models

produced a more consistent tropical Pacific winter mean SST distribution, Pacific jet model biases would be more consistent. The same relationship is not as clear in the Atlantic (2.6b), though it is noteworthy that the portion of zonal wind bias that is related to ENSO-like mean state biases (the circles in 2.6b) do generally align along the "Group 1, Group 2" axis. This suggests that tropical Pacific mean state biases may be responsible for some portion of the bias of the Atlantic jet as well.

In order to further confirm and detail the relationship of the Pacific modeled ENSO-like tropical mean state and mid-latitude zonal wind biases, we examine the spatial structure of zonal wind variations associated with *temporal* ENSO variations in the observed record, and compare these results with the results of the MCA above. One commonly-used metric for defining ENSO is the cold tongue index (CTI; Zhang et al. (1997)), defined by the sea surface temperature (SST) anomaly pattern over the eastern equatorial Pacific (6°S - 6°N, 180° - 90°W). Fig. 2.9 shows the regression of the reanalysis wintertime (NDJFM; annually resolved) zonal wind and wintertime SST fields onto the reanalysis wintertime CTI for 1950-2009. The regression therefore depicts the average observed patterns of wintertime SST and upper-level zonal wind associated with a positive CTI. Fig. 2.9b shows the canonical positive ENSO (El Niño) SST signal of warming in the eastern equatorial Pacific and Fig. 2.9a shows the wintertime zonal wind teleconnection pattern associated with El Niño SST anomalies. The positive phase of ENSO is associated with increased wind speeds within a subtropical band (15°-30°N) stretching from the dateline to approximately 90°W.

The normalized projection of the observed ENSO teleconnection pattern (Fig. 2.9a) onto the primary and secondary modes of variability from the reanalysis (EOF 1-2, Fig. 2.2) is shown by

the open diamonds added to Fig. 2.6. In the Pacific region (Fig. 2.6a), these diamonds also fall along nearly the same axis as inter-model variations in jet stream biases and the heterogeneous wind pattern produced by MCA. The near-alignment of these different variables shows that they all project onto a similar combination of EOF 1-2. Thus, it is even more likely that the ENSO-like state of modeled SSTs explains inter-model differences in the bias of NH jet streams in the Pacific. While the link between Atlantic jet biases and ENSO is weaker (2.6b), inter-model variations do lie along the same axis as the ENSO teleconnection pattern. Therefore, it seems that model biases in the portrayal of the Atlantic jet are also affected by tropical Pacific mean state biases.

To further confirm the results of MCA, the mean winter upper-level wind field is regressed onto the mean winter CTI for each model, with results shown in Fig. 2.10. The results of this regression analysis look remarkably similar to the results of MCA, and are correlated with the heterogeneous wind field (Fig. 2.8a) at r = 0.98 and with the grouped model bias pattern (Fig. 2.7) at r = 0.71. This confirms that jet stream biases across the 17 GCMs are related to the ENSO-like biases in tropical Pacific SST in these models. However, a comparison between Fig. 2.10 and Fig. 2.9a shows that the jet stream bias pattern associated with ENSO-like SST biases in GCMs does not completely resemble the observed ENSO teleconnection pattern (r = 0.46). Additional thoughts on this issue are found in Section 2.4.

To quantify how much inter-model variance is explained by the ENSO-like pattern identified by MCA, the SST expansion coefficient (i.e. the left singular vector) of the first mode of MCA covariability is used as a predictor of inter-model variance of upper-level winds, allowing the determination of what percentage of the inter-model variance of upper-level winds is explained

by GCM SST biases. The result of this analysis, shown in Fig. 2.11, finds that ENSO-like SST biases explain 21% of the NH inter-model variance of mid-latitude jet stream portrayal on average, with significantly more variance explained in the central subtropical Pacific and eastern subtropical Atlantic. Fig. 2.11b shows that while SST biases do not explain all of the inter-model variance in upper-level winds, they do explain a substantial portion, especially in the Pacific.

2.3.4 GCM portrayal of jet variability

To complete this analysis of NH jet stream portrayal, temporal variability of the upper-level winds is also considered. EOF/PC analysis is used to determine the primary and secondary modes of variability associated with the Pacific and Atlantic jets for each model. The same methodology is used as for the reanalysis data (Section 2.3.1). EOF/PC 1 and 2 are well separated for all models.

Figure 2.12 shows the normalized projection of the first two EOFs of each model onto the first two EOFs of the reanalysis data (a. Pacific, b. Atlantic). Asterisks (Crosses) indicate the value of the projection of EOF 1 (EOF 2) of a given model onto EOF 1 (EOF 2) of the reanalysis. For instance, an asterisk located at (1,0) would describe an exemplary model's depiction of EOF 1 that is completely explained by reanalysis EOF 1 and not explained by reanalysis EOF 2. It is important to note that the sign of a given mode is arbitrarily determined and therefore the polarity is assigned based upon the convention established by reanalysis EOF 1-2 (Fig. 2.2).

Most points cluster near (0,1) or (1,0), indicating that GCMs are successfully replicating the two dominant modes of variability. There are only 3 outlier points: two for the Atlantic and one for the Pacific. The Atlantic outliers are EOF 1 and 2 from Model 1 (INGV-SXG), and indicate the reversal of EOF 1 and 2 in that model (not shown). Because EOF 1 and 2 explain 15% and 14%

of the variability of the Atlantic upper level winds respectively, this reversal is not a serious flaw in the modeled variability. For the one outlier in the Pacific (EOF 2 from Model 16, GISS-ER) it is found that EOF 2 and EOF 3 are reversed (not shown), another minor flaw since these modes explain 11% and 9% of the variability respectively. Therefore, all 17 models do a good job of replicating the two dominant modes of variability. Even the outliers have the correct structures represented in the wrong order. In fact, this variability appears to be more consistently replicated than the mean state of the jets in GCMs (Fig. 2.6).

Because the location of the perturbation wind speeds associated with the dominant modes of variability is located nearby the jet exit region (see, e.g., Fig. 2.2), a measure of the longitude of the jet exit region and the longitude of wind speed anomalies associated with EOF 1-2 is used to find a functional relationship between jet mean state and variability.

A regression analysis, shown in Fig. 2.13 examines the relationship between the modeled modes of variability and modeled mean state of the Atlantic and Pacific jets. The longitude of the maximum wind perturbation associated with EOF 1-2 is regressed onto the longitude of the jet exit region for each model, as defined by the local minimum of the zonal gradient of the mean winter zonal wind from each model. Model 16 (GISS-ER) is removed from the analysis of Pacific EOF 2 and Model 1 (INGV-SXG) is removed from the analysis of Atlantic EOF 1-2 because they do not correctly represent their respective EOFs (as shown in Fig. 2.12).

For the Pacific jet, the longitude of the maximum value of EOF 1-2 is highly correlated with the longitude of the jet exit region (r = 0.88, r = 0.68), shown in Fig. 2.13a and 2.13b (open circles show results from reanalysis dataset). The $y = x$ line is also shown for the Pacific, which indicates

the line the regression would follow if EOF 1-2 were located exactly at the longitude of the jet exit region. Most models correctly portray the maximum wind perturbation to be located immediately downstream of the jet exit region.

Figures 2.13c and 2.13d show the regression analysis for the Atlantic jet, which does not display a similar strong connection (r = 0.41, r = 0.43). The models all portray the maximum wind perturbation too far downstream for EOF 1 and most models portray the maximum wind perturbation too far upstream for EOF 2. Overall, there does not seem to be a link between the longitude of the mean state and variability for the Atlantic region, possibly because of the added complexity due to the southeast-northwest tilt of the jet in this region.

There is a robust correspondence between the Pacific jet mean state and its variability, but not the Atlantic jet mean state and variability. When these results are repeated using GCM 21st century A1B projections (not shown), this correspondence (or lack thereof in the Atlantic) does not change. Therefore, the Pacific jet exit region is critically related to the longitudinal position of EOF 1 and 2, signifying that a correct characterization of the mean state of the Pacific jet stream is vital to producing an accurate portrayal of the variability of that jet stream.

2.4 Conclusions

This study has focused on determining the reliability and robustness of non-zonally averaged NH jet stream portrayal in 17 GCMs from the CMIP3 dataset. This work is motivated by previous studies showing that GCM projections of 21st century jet stream winds are related to biases in 20th century jet stream portrayal (Kidston and Gerber, 2010). The results presented in this chapter

encourage targeted improvement of GCM jet stream portrayal, which is an important step toward assessing climate change impacts at a variety of scales.

Examination of ensemble mean biases of upper-level zonal winds suggests that the modeled Atlantic jet is too zonally extended and located too far equatorward compared to the reanalysis. The ensemble mean Pacific jet is less biased than the Atlantic jet, but only because model agreement is much lower and biases in individual models cancel in the ensemble mean. Mean winter biases in both basins are significant compared to the observed variability of the upper-level zonal winds.

MCA and regression analysis are used in tandem to show that the NH biases in upper-level winds are strongly related to an ENSO-like pattern in winter mean tropical Pacific SSTs. Throughout the analysis we have implicitly assumed that tropical SSTs are responsible for forcing mid-latitude winds, suggesting that the variation in models' portrayal of the tropical Pacific mean state contributes to the bias of the mid-latitude large-scale circulation. However, it is important to note that the reverse scenario is also possible. Recent studies have shown that variations in mid-latitude and subtropical winds may also conspire to produce tropical Pacific ENSO variations, as evidenced by the seasonal footprinting mechanism examined in Vimont et al. (2001). It is possible that this causal mechanism (from mid-latitude to the tropics) would also work in linking mid-latitude wind biases to biases in tropical Pacific SST. While the present study does not resolve that causality, the similarity between the spatial structure of ENSO's teleconnection in the observed record to the model bias (Fig. 2.6a) suggests that biases in the tropical Pacific are influencing mid-latitude zonal wind biases.

Temporal variability of the upper-level zonal winds is accurately modeled in nearly all 17 GCMs. Furthermore, it is shown that in the Pacific, biases that do exist in models' portrayal of EOFs 1 and 2 are strongly linked to the modeled longitude of the jet exit in the Pacific region. This result is particularly encouraging because it implies that an improved characterization of the mean state of the Pacific jet will also positively impact the modeled variability.

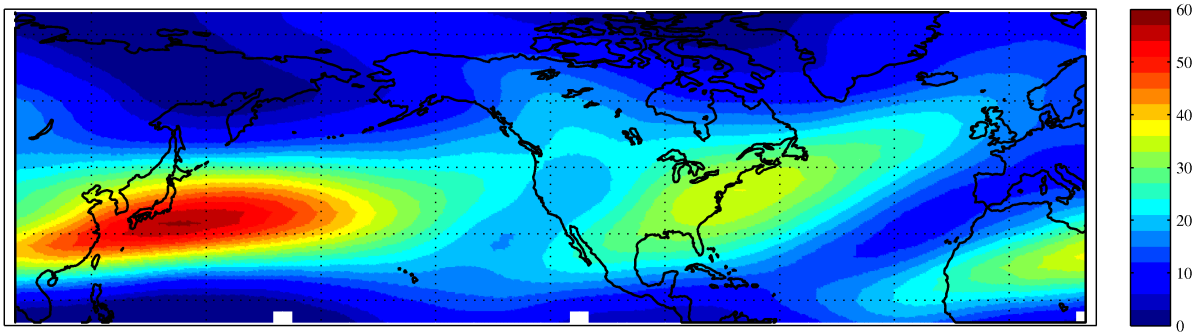

Figure 2.1 Reanalysis zonal wind (m s^{-1}) at 300 hPa for NH winter (November-March) 1979–1999.

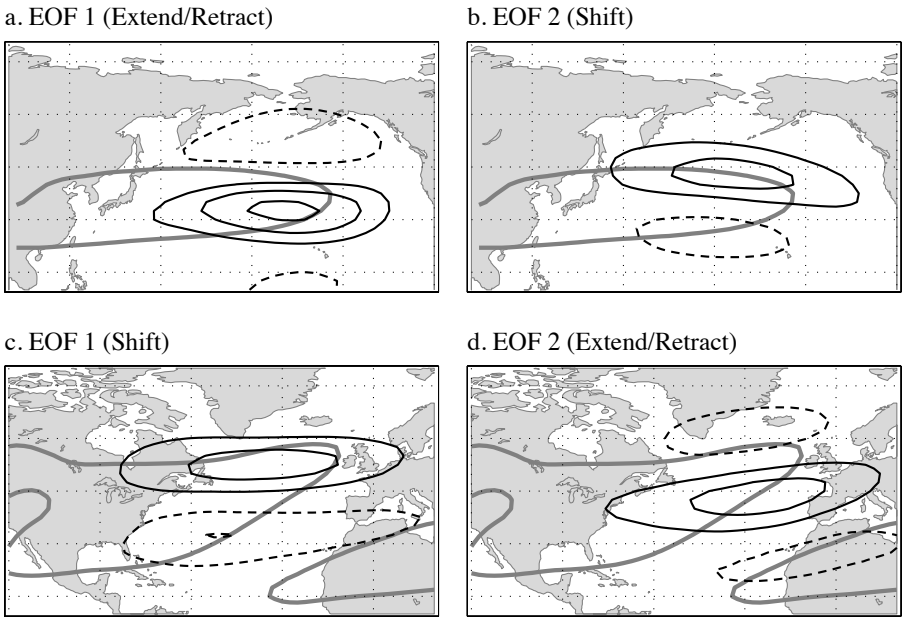

Figure 2.2 EOFs of the 300 hPa midlatitude zonal wind field (20°–80°N) regressed onto the total 300 hPa zonal wind field (0°–80°N). Solid (dashed) black lines represent positive (negative) perturbation isotachs, contoured every 4 m s^{-1} with the zero line removed for (a) Pacific basin EOF 1 (Extend/Retract), (b) Pacific basin EOF 2 (Shift), (c) Atlantic basin EOF 1 (Shift), (d) Atlantic basin EOF 2 (Extend/Retract). Gray contours show the 20 (30) m s^{-1} isotach of the mean 300 hPa zonal wind for the Atlantic (Pacific) basins.

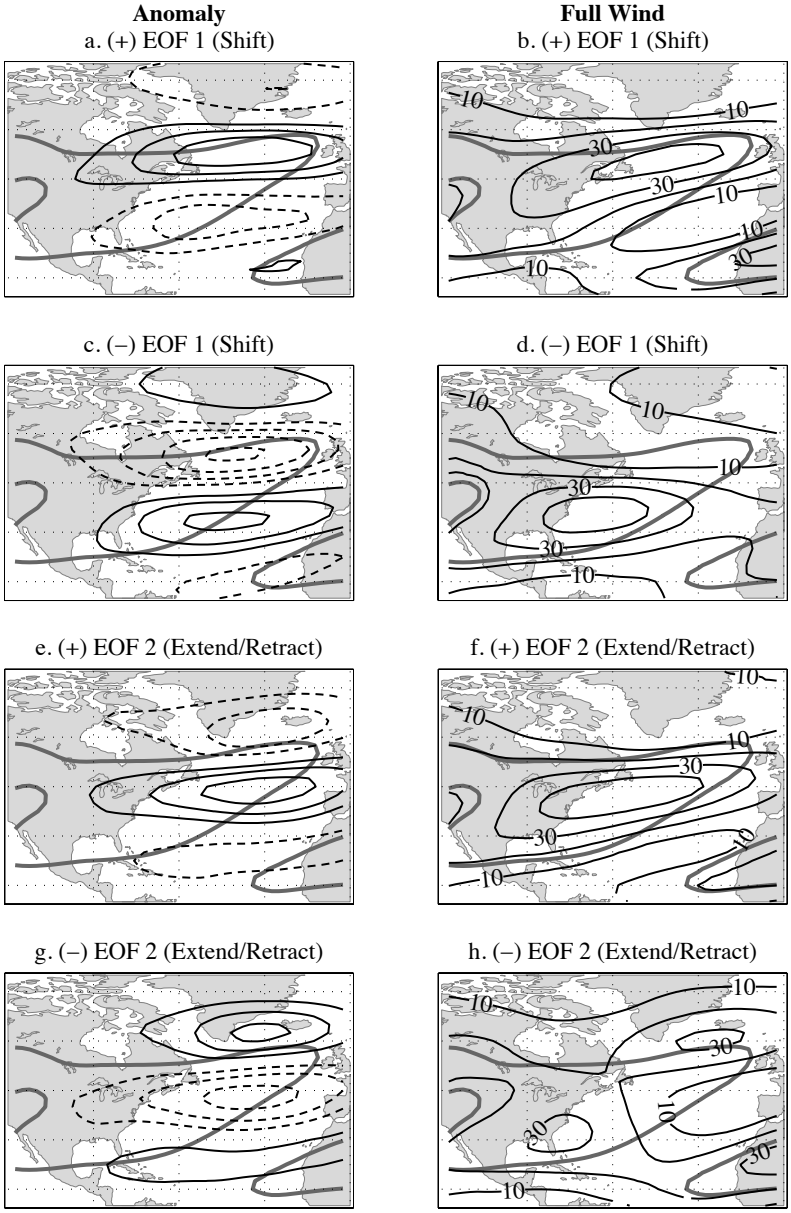

Figure 2.3 Composites of maximum variability of the 300 hPa zonal wind field in the Atlantic. Gray contours show the 20 m s^{-1} isotach of the mean 300 hPa zonal wind for the Atlantic. Solid (dashed) black lines in the left column indicate positive (negative) perturbation isotachs, contoured every 5 m s^{1} with the zero line removed. The right column shows perturbation isotachs added to the climatology in units of m s^{-1} for (a)-(b) 1st principal component (PC) greater 1 standard deviation (1*σ), (c)-(d) 1st PC less than -1*σ, (e)-(f) 2nd PC greater than 1*σ, (g)-(h) 2nd PC less than -1*σ.

a. Ensemble Mean Bias

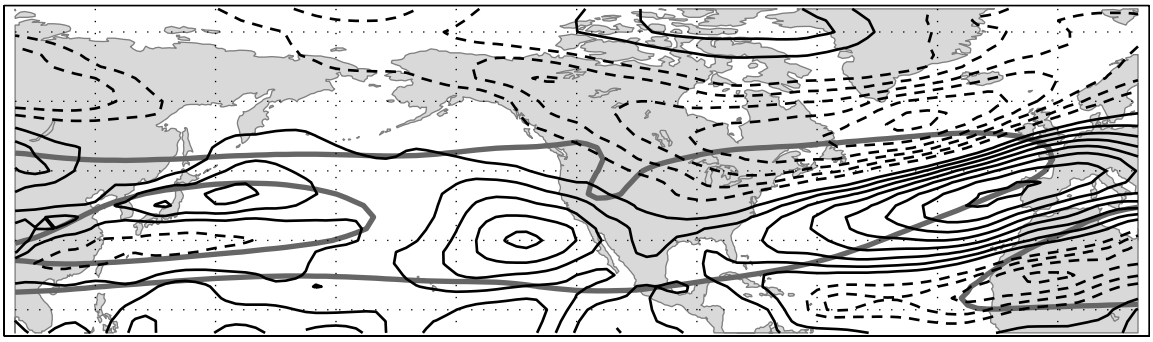

b. Model Standard Deviation of Bias

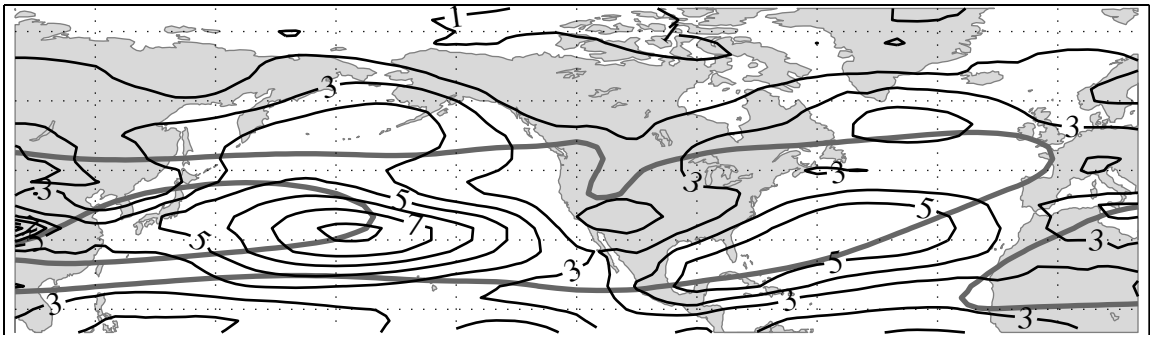

Figure 2.4 (a) Ensemble mean model bias and (b) Standard deviation of models about the ensemble mean for the 17 GCMs under consideration [m s^{-1}]. Solid (dashed) black contours in (a) represent positive (negative) values of ensemble mean bias, contoured every 1 m s^{-1} with the zero line removed. The gray contours show the 20, 40 m s^{-1} isotachs of the model mean winter 300 hPa zonal wind

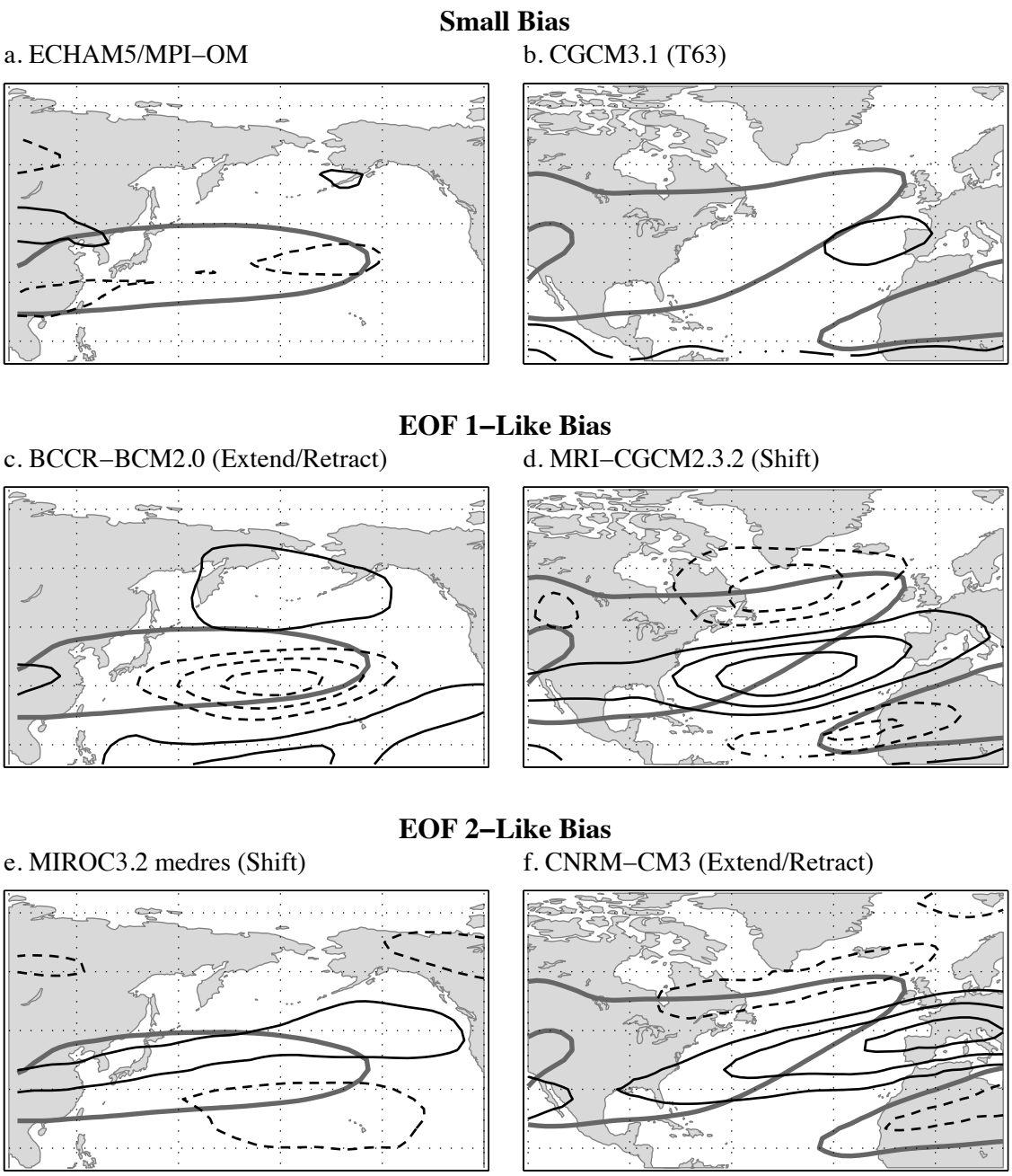

Figure 2.5 Solid (dashed) black contours show the positive (negative) bias of the 300 hPa zonal wind, contoured every 4 m s^{-1} with the zero line removed for (a) Model 5: ECHAM5/MPI-OM, (b) Model 8: CGCM3.1 (T63), (c) Model 7: BCCR-BCM2.0, (d) Model 11: MRI-CGCM2.3.2, (e) Model 10: MIROC3.2 (medres), (f) Model 9: CNRM-CM3. Gray contours show the 20 (30) m s^{-1} isotachs of the 300 hPa zonal wind for the Atlantic (Pacific) basin.

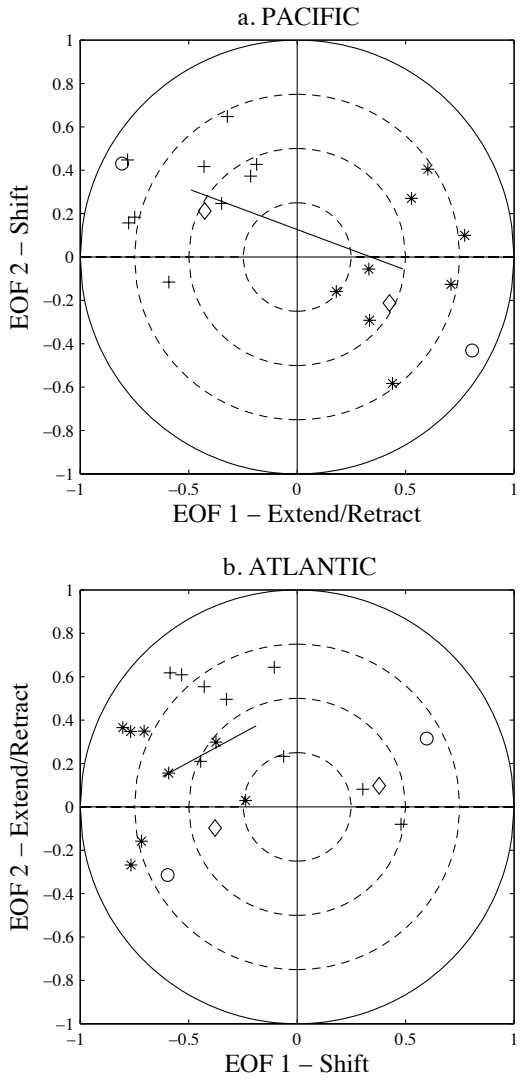

Figure 2.6 Normalized projection of the model bias of the 300 hPa zonal wind onto EOF 1 and 2 from the reanalysis for the (a) Pacific and (b) Atlantic basins. Models designated by crosses (+) are part of Group 1 and models designated by asterisks (*) are part of Group 2. Dashed circles indicate lines of constant correlation at r = 0.25, 0.5, and 0.75. The black line connects the average Group 1 projection to the average Group 2 projection. Open circles (diamonds) show the values of the normalized projection of the heterogeneous wind pattern shown in Fig. 2.8a (ENSO teleconnection pattern shown in Fig. 2.9a) onto EOF 1 and 2.

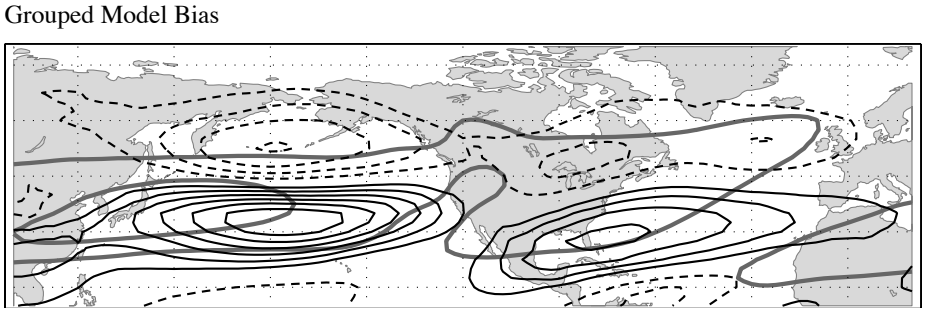

Figure 2.7 Solid (dashed) black lines show the positive (negative) model bias of the 300 hPa zonal wind, contoured every 1 m s^{-1} with the zero line removed for ($Group\ 2 - Group\ 1$), where models are separated into Group 1 (models 1, 5, 7, 8, 9, 10, 12, 13, 17) and Group 2 (models 2, 3, 4, 6, 11, 14, 15, 16), based upon their delineation in Figure 6, as described in the text. Gray contours show the 20, 40 m s^{-1} isotachs of the model mean 300 hPa zonal wind.

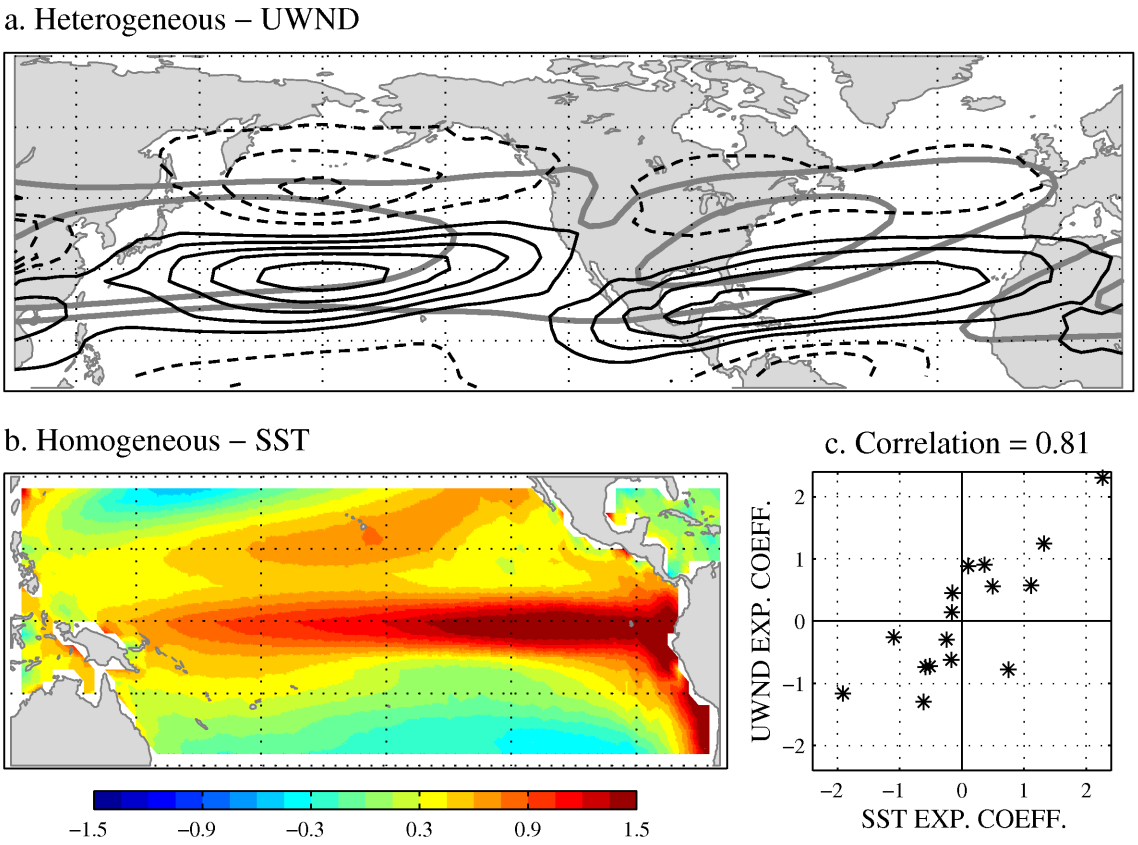

Figure 2.8 Results of MCA of tropical Pacific SSTs and mid-latitude 300 hPa zonal wind. (a) Heterogeneous wind regression map, (b) Homogeneous SST regression map, (c) Scatter plot of the wind and SST expansion coefficients. Solid (dashed) black contours in (a) represent positive (negative) perturbation isotachs, contoured every 1 m s^{-1} with the zero line removed. Gray contours in (a) show the 20, 30 m s^{-1} isotachs of the model mean 300 hPa zonal wind.

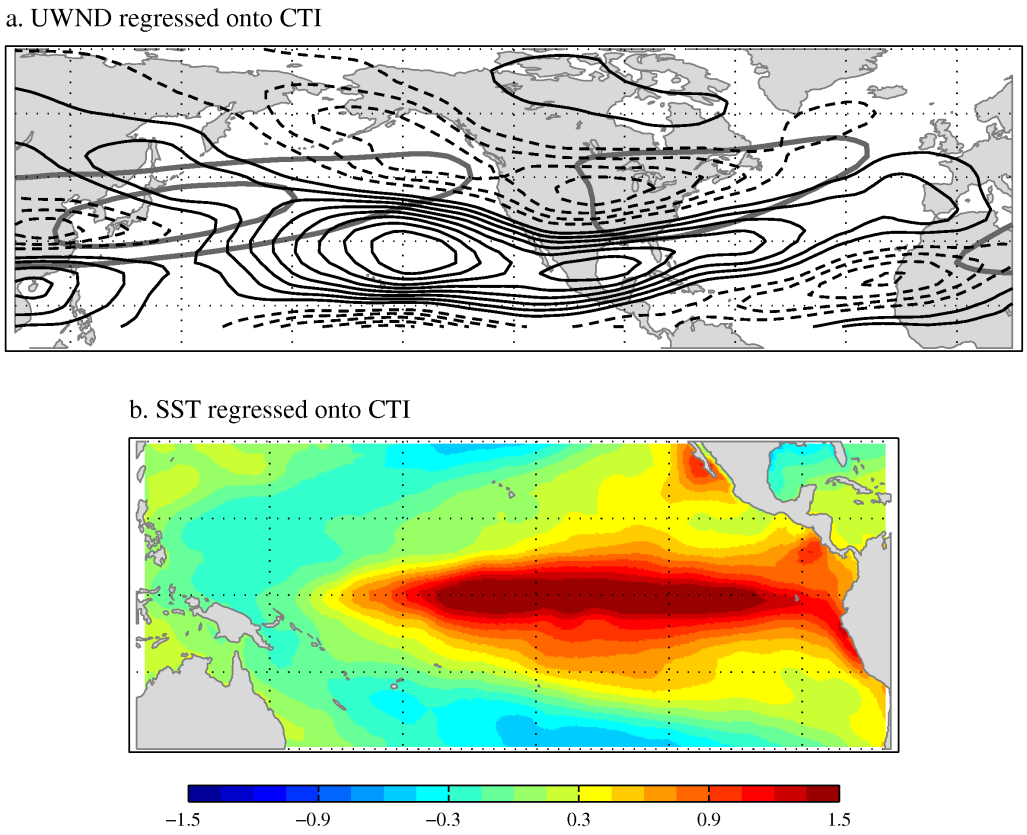

Figure 2.9 ENSO mid-latitude wind teleconnection (1950-2009) shown by: (a) Observed mean winter 300 hPa zonal wind regressed onto the mean winter CTI and (b) mean winter tropical Pacific SST regressed onto the mean winter CTI. Solid (dashed) black contours in (a) represent positive (negative) perturbation isotachs, contoured every 0.5 m s^{-1} with the zero line removed. Gray contours represent the 20, 30 m s^{-1} isotachs of the 300 hPa mean zonal wind.

Model CTI regressed onto Model 300 hPa Zonal Wind

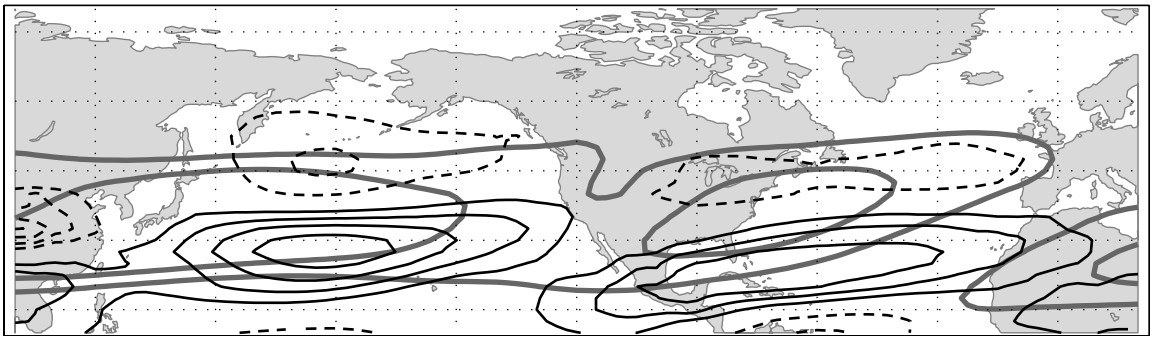

Figure 2.10 Modeled mean winter cold tongue index (CTI) for each model regressed onto the modeled mean winter 300 hPa zonal wind field. Solid (dashed) black lines indicate positive (negative) perturbation isotachs, contoured every 1 m s^{-1} with the zero line removed. Gray contours show the 20, 30 m s^{-1} isotachs of the model mean 300 hPa zonal wind.

a. Raw Inter−model Variance

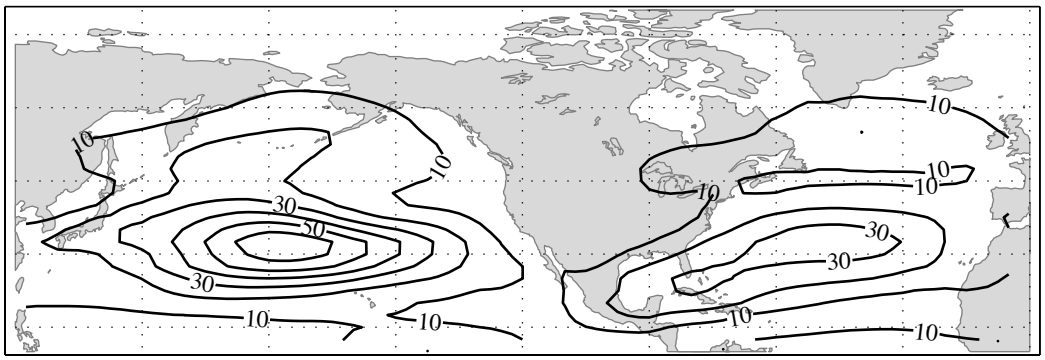

b. Variance explainted by MCA1

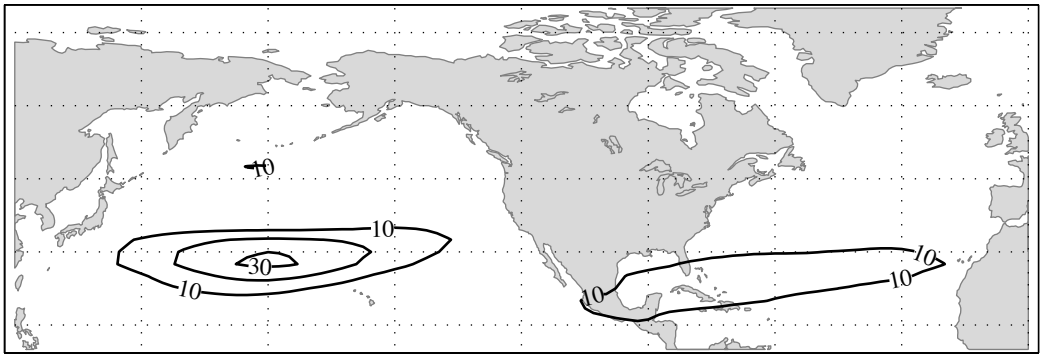

Figure 2.11 (a) Total inter-model variance of the mean winter 300 hPa zonal wind and (b) Inter-model variance of the mean winter 300 hPa zonal wind explained by the SST expansion coefficient of the first mode of MCA covariability. Variance is expressed in units of $m^2\ s^{-2}$ and contoured every 10 $m^2\ s^{-2}$

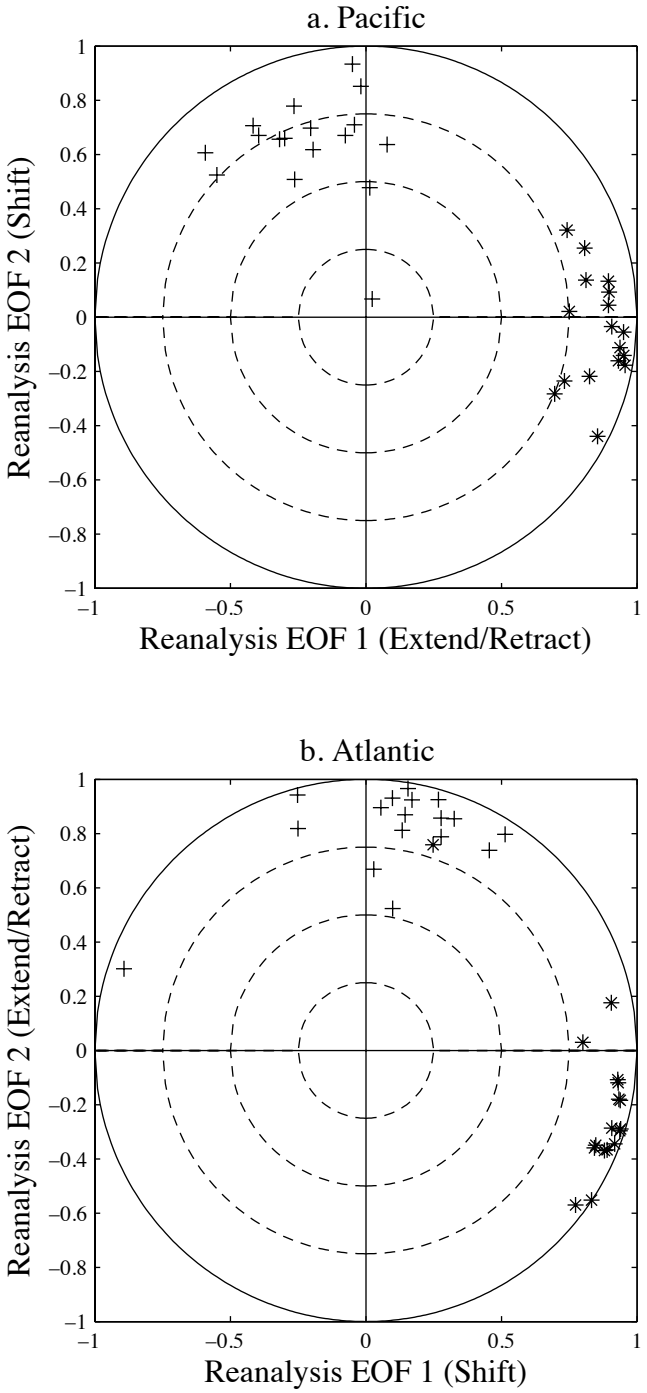

Figure 2.12 Scatter plot of the normalized projection of each model's PC/EOF 1-2 onto the corresponding reanalysis PC/EOF 1-2 for (a) the Pacific, (b) the Atlantic. EOF 1 is indicated by asterisks (*) and EOF 2 is indicated by crosses (+). Dashed circles indicate lines of constant correlation at r = 0.25, 0.5, and 0.75.

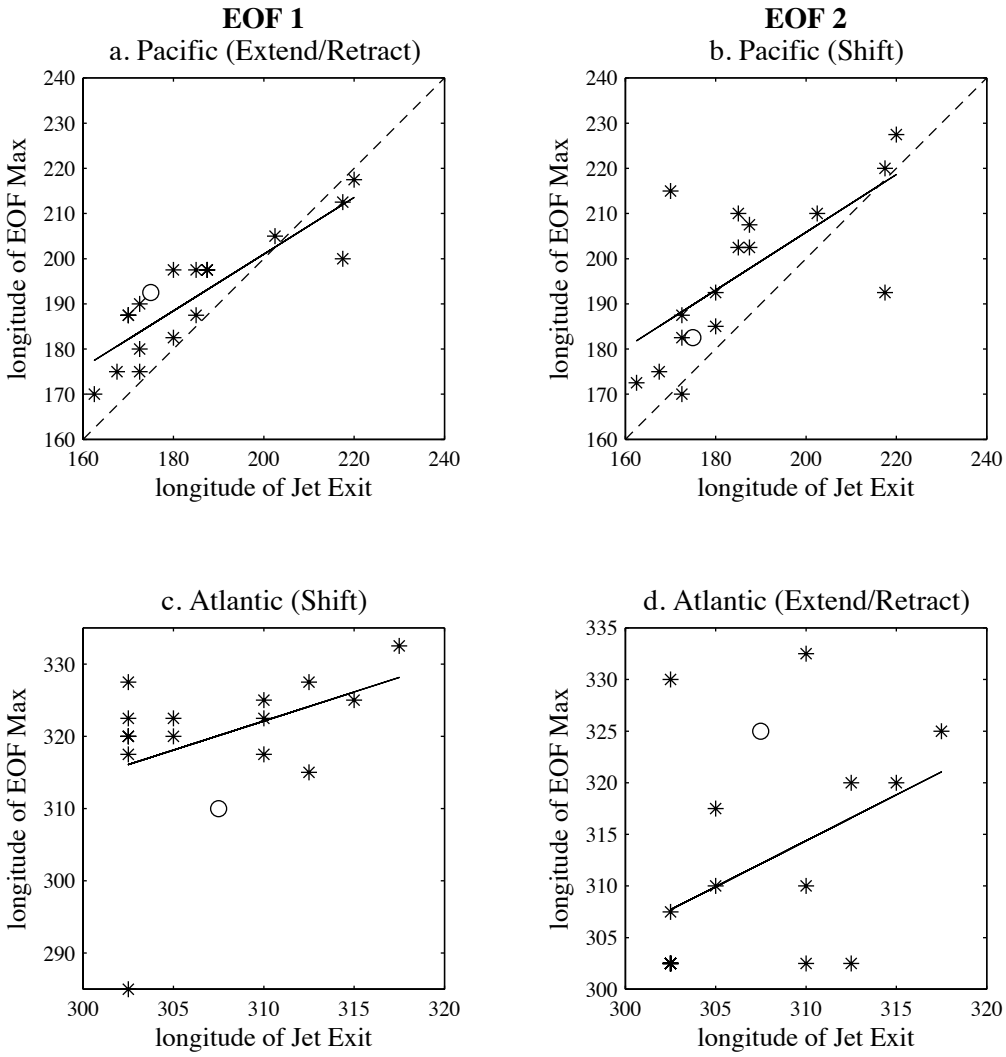

Figure 2.13 Longitude of the maximum wind perturbation associated with EOF 1/2 regressed onto the longitude of the jet exit region in each model for (a) Pacific EOF 1 (Extend/Retract), (b) Pacific EOF 2 (Shift), (c) Atlantic EOF 1 (Shift), (d) Atlantic EOF 2 (Extend/Retract). Open circles represent reanalysis data and the dashed line shows $y = x$.

Table 2.1 CMIP3 Models

Number	*Model*	*Modeling Group*	*Reference*
1	INGV-SXG	Instituto Nazionale di Geofisica e Vulcanologia	Gualdi et al. (2006) and Gualdi et al. (2008)
2	MIROC3.2 (hires)	Center for Climate System Research (the University of Tokyo), National Institute for Environmental Studies, and Frontier Research Center for Global Change (JAMSTEC)	Hasumi and Emori (2004)
3	CSIRO-Mk3.0	Commonwealth Scientific and Industrial Research Organisation (CSIRO) Atmospheric Research	Gordon et al. (2002)
4	CSIRO-Mk3.5	Commonwealth Scientific and Industrial Research Organisation (CSIRO) Atmospheric Research	Gordon et al. (2002)
5	ECHAM5/MPI-OM	Max Planck Institute for Meteorology	Jungclaus et al. (2006)
6	GFDL-CM2.0	U.S. Department of Commerce/National Oceanic and Atmospheric Administration (NOAA)/Geophysical Fluid Dynamics Laboratory	Delworth et al. (2006) and Gnanadesikan et al. (2006)
7	BCCR-BCM2.0	Bjerknes Center for Climate Research	http://www.bjerknes.uib.no/
8	CGCM3.1 (T63)	Canadian Centre for Climate Modeling and Analysis	Flato et al. (2000) and http://www.ec.gc.ca/ccmac-cccma
9	CNRM-CM3	Météo-France/Centre National de Recherches Météorologiques	http://www.cnrm.meteo.fr/scenario2004/paper_cm3.pdf
10	MIROC3.2 (medres)	Center for Climate System Research (the University of Tokyo), National Institute for Environmental Studies, and Frontier Research Center for Global Change (JAMSTEC)	Hasumi and Emori (2004)
11	MRI-CGCM2.3.2	Meteorological Research Institute	Yukimoto et al. (2006)
12	FGOALS-g1.0	State Key Laboratory of Numerical Modeling for Atmospheric Sciences and Geophysical Fluid Dynamics (LASG)/Institute of Atmospheric Physics	Yu et al. (2002) and Yu et al. (2004)
13	CGCM3.1 (T47)	Canadian Centre for Climate Modeling and Analysis	Flato et al. (2000) and http://www.ec.gc.ca/ccmac-cccma
14	ECHO-G	Meteorological Institute of the University of Bonn, Meteorological Research Institute of KMA, and Model and Data group	http://mad.zmaw.de/Models/Modelliste1_neu.html
15	GISS-AOM	NASA Goddard Institue for Space Studies	Russell et al. (1995) and Lucarini and Russell (2002)
16	GISS-ER	NASA Goddard Institue for Space Studies	Schmidt et al. (2006)
17	INM-CM3.0	Institute for Numerical Mathematics	Volodin and Diansky (2004) and Galin et al. (2003)

Chapter 3

21st Century Projections of Jet Stream Structure

3.1 Background

Understanding how the jet streams will change in the future is of primary importance in the assessment of anthropogenic climate change impacts. Jet stream position and intensity affect regional climates across the mid-latitudes and also are linked to the mid-latitude storm tracks.

As described in Chapter 2, the portrayal of jet stream winds in CMIP3 GCMs still lacks consensus with regard to modeled 20th century jet stream structure, especially in the Northern Hemisphere (Lorenz and DeWeaver, 2007; Kushner et al., 2001; Kidston and Gerber, 2010; Woollings and Blackburn, 2012; Yaocun and Daqing, 2011; Ihara and Kushnir, 2009). The previous analysis finds significant biases in the upper-level wintertime zonal wind compared to the observed variability of upper-level winds. These wind biases are strongly related to an ENSO-like structure of wintertime tropical Pacific SST biases that explains 21% of the total NH inter-model variance of the mid-latitude jet stream.

As a complement to the 20th century analysis, modeled NH jet streams are investigated in order to discover what underlies the significant inter-model variability among 21st century projections and is organized as follows. Section 3.2 outlines the GCM data used in this study. Results of

a detailed analysis of 21st century jet streams in GCM simulations are presented in Section 3.3. These results include an examination of inter-model variations related to both internal modes of variability and tropical SSTs. The main analysis tool used is maximum covariance analysis (MCA). Conclusions for Chapter 3 are found in Section 3.4.

3.2 Data and Methods

The present study investigates 21st century NH jet stream structure in 17 GCMs from the World Climate Research Programme's (WCRP's) Coupled Model Intercomparison Project phase 3 (CMIP3) multi-model dataset (Meehl et al., 2007). Table 2.1 lists the models included in this study. These particular models are chosen because they provide the daily-resolved data required for this study.

The 20th century GCM data is produced by the climate of the 20th century experiment (20c3m) and the 21st century data employs the A1B scenario from the special report on emissions scenarios (Nakicenovic, 2000, SRES). The A1B scenario models the 21st century as a time of rapid economic growth and the rapid introduction of new energy technologies that are balanced between fossil fuel and non-fossil fuel sources. Population peaks mid-century in the A1B scenario, making it one of the mid-range scenarios used in the CMIP3 model experiments.

Analysis is performed on daily 300 hPa and 700 hPa zonal wind and monthly sea surface temperature (SST) for the change from the 20th century to the 21st century. Daily zonal wind data are smoothed using a 5 day running mean for the period encompassing November 1 through March 31st of each winter from November 1979 to March 1999 and November 2081 to March 2099 (with

leap days removed). The 17 GCMs vary in resolution from 1.125° latitude x 1.125° longitude (Model 1 - INGV-SXG) to 4° latitude x 5° longitude (Model 17 - INM-CM3.0). To facilitate a straightforward comparison, each model is linearly interpolated to 2.5° latitude x 2.5° longitude resolution.

To create the mean winter zonal wind (SST) for the 20th and 21st centuries, the smoothed (monthly) data were averaged over NDJFM and over all 20 years of each data period. The seasonal cycle of zonal wind is created by averaging each smoothed day (i.e. pentad) over all 20 boreal winter seasons. Smoothed daily wind data (with the seasonal cycle removed) are used to perform EOF/PC analysis.

3.3 Results and Discussion

3.3.1 300 hPa Zonal Wind Change from the 20th Century to the 21st Century

To understand why GCMs do not project a consistent representation of 21st century NH jet stream structure, the ensemble mean and standard deviation of the change in zonal wind from the 20th century to the 21st century (1980 – 1999 to 2081 – 2100, from here on referred to as the "change in zonal wind") are inspected and then examined in the context of internal and external system forcings.

Although the present study does not focus on a zonal mean perspective of wind speed changes in GCM projections, sectorial zonal means of the Pacific (100°E - 300°E) and Atlantic (240°E - 360°E) regions are shown in Fig. 3.1 to connect the present study with the larger background of work on this topic. Figs. 3.1a and 3.1b show the mean model 20th century winter (NDJFM, 1980

– 1999) Pacific and Atlantic zonal mean jets. Zonal mean winds are maximized in the upper troposphere and are stronger in the Pacific than in the Atlantic. The mean winter westerlies penetrate into the lower troposphere in both regions.

Figures 3.1c and 3.1d also include the ensemble mean change of the winter zonal mean zonal wind. The two regions show similar structures of change that are characterized by an intensification of upper-level wind speeds and a northward (poleward) shift of the low-level winds associated with the jet stream. This increase in upper winds is consistent with the theorized direct response to anthropogenic climate change described in Section 1. The standard deviation of the change of the winter zonal mean wind from the ensemble mean (Figs. 3.1e and 3.1f) is relatively small at upper-levels and large at lower-levels compared to the ensemble mean change (Figs. 3.1c and 3.1d). This suggests that the upper-level jet intensification in the region of maximum winds is much more robust than the low-level poleward shift of the jet among models. Because the maximum wind speeds are found in the upper-levels of the troposphere, the present study will further analyze the modeled 300 hPa zonal winds in order to determine what underlies inter-model discrepancies in 21st century projections. A brief comparison at 700 hPa is found in Fig. 3.8.

The non-zonally averaged ensemble mean change in the winter 300 hPa zonal wind is shown in Fig. 3.2a. The 20th century ensemble mean zonal wind at 300 hPa is superimposed in gray. The 20th century climatology shows that the wintertime zonal wind is maximized in the Pacific and Atlantic basins, with the Pacific jet extending from East Asia across the Pacific basin and the Atlantic jet extending from the central continental United States toward the west coast of Europe, tilting northeastward across the Atlantic basin.

In the Pacific region, the ensemble mean change in zonal wind is largest on the poleward flank of the Pacific jet (Fig. 3.2a) and accompanied by a region of decreasing zonal winds in the vicinity of the jet entrance region. This asymmetric pattern looks different than the theorized poleward shift of the jet because the decrease in zonal wind is collocated with the jet axis, suggesting a poleward expansion and slight weakening of the Pacific jet in the ensemble mean. Wind speeds also increase over the eastern subtropical Pacific. In the Atlantic region, zonal winds are projected to increase poleward, equatorward, and downstream of the jet core, suggesting an overall expansion of the Atlantic jet in the ensemble mean (Fig. 3.2a).

It is interesting to note that in contrast to the direct climate change signal of increasing mid-latitude upper-level winds (i.e. Fig. 3.1), 300 hPa ensemble mean zonal winds show a decrease in the core of both the Pacific and Atlantic jets. Increasing 300 hPa ensemble mean zonal winds are located primarily in the jet exit regions as well as on the meridional flanks of the jets. When zonally averaged, this pattern does indicate strengthening mid-latitude upper-level winds on average because winds are strengthening nearly everywhere except the jet core. This is one instance in which a zonal mean perspective is somewhat misleading.

The problem is that the 17 GCMs under consideration are not consistent with regard to the changes in jet stream structure in the 21st century. The standard deviation of the model change in zonal wind (Fig. 3.2b) shows that in many areas of the globe, the magnitude of the model standard deviation of wind speed change is the same or higher than the ensemble mean itself, indicating that models do not hold a unified view of the future. In particular, the standard deviation is large in the vicinity of the Pacific and Atlantic jet exit regions.

Internal jet variability is also maximized in the jet exit region, suggesting a link between model differences in changes in zonal wind and the internal modes of jet variability. Previous studies have also suggested this link; it has been hypothesized that anthropogenic climate change may project onto the natural internal modes of variability (Ring and Plumb, 2008; Gerber et al., 2008a). A normalized projection of each model's change in zonal wind at 300 hPa and 700 hPa onto EOF 1 and 2 of the 20th century zonal wind at the same level and in the same model is used to quantify the relationship between wind speed changes and internal variability. EOF 1-2 polarity is selected to match the analysis in Chapter 2. This analysis is done separately for the Pacific (100°E - 120°W) and Atlantic (120°W - 20°E) regions, shown for 300 hPa in Figs. 3.3a and 3.3b and for 700 hPa in Figs. 3.3c and 3.3d. The position of each point with respect to the x-axis (y-axis) shows the value of each models projection onto EOF 1(2). Chapter 2 (Fig. 2.12) shows that modeled EOF 1-2 are accurate in nearly all GCMs included in this study. In both the Pacific (Figs. 3.3a and 3.3c) and the Atlantic (Figs. 3.3b and 3.3d), at 300 hPa and 700 hPa, the values of the normalized projection are spread more along the x-axis than the y-axis, indicating that EOF 1 explains more variation in wind speed change among models than EOF 2. While 300 hPa and 700 hPa show somewhat different patterns of projection, there is no consistent projection of the change in wind onto either sign of the internal modes of variability at either level.

This analysis technique also makes it possible to quantify the relationship between the modeled change in winds and the predicted poleward shift of the jet, which can be described mathematically as $-\frac{du}{dy}$ for small shifts (Kushner et al., 2001). It is expected that the projection of the change in zonal wind onto the poleward shift of the jet will be similar to the projection onto the internal

modes of variability because the secondary (primary) mode of variability of the Pacific (Atlantic) jet is qualitatively similar to a poleward shift of the jet (Fig. 2.2). Therefore, the y-axis (x-axis) of Fig. 3.3a and 3.3c (3.3b and 3.3d) can be replaced with $-\frac{du}{dy}$ to see if a poleward shift is a better predictor of zonal wind changes than EOF 1-2. This analysis also shows the absence of a robust projection of the change in wind onto $-\frac{du}{dy}$ for each basin (results not shown).

3.3.2 Relationship between wind speed changes and tropical Pacific SSTs - MCA

Based upon the results of Chapter 2, which found that mean winter tropical Pacific sea surface temperature (SST) variations explain much of the inter-model jet bias in 20th century, it seems possible that tropical Pacific SST changes influence modeled wind speed changes more than the internal modes of atmospheric variability. Maximum covariance analysis (MCA) is used to investigate this relationship.

MCA is used here to assess the dominant patterns of covariability between tropical SSTs and the change in zonal wind from the 20th to the 21st century across the same 17 GCMs. This technique identifies pairs of patterns that maximize the squared covariance between two variables: in this case the mid-latitude 300 hPa zonal wind speed change (100°E – 20°W, 10°N – 80°N) and the tropical Pacific SST change (30°S – 30°N, 120°E – 290°E). The covariance is identified across a given sampling dimension. Typically sampling is performed across time, but in this case sampling is done across the 17 GCMs to identify structures linked to model discrepancies, as in Chapter 2. Again, it is important to note that because this MCA analysis samples across model space instead of across time, ENSO-like SST change patterns that are identified are not equivalent

to inter-annual variability in any model. Instead, these ENSO-like patterns of SST change show the change in the winter mean state of the tropical Pacific from the 20th century to the 21st century that is associated with a given mode of inter-model covariability.

MCA is performed three times for the 300 hPa zonal wind change, with the results shown in Figs. 3.4 to 3.6. Table 3.1 includes the details of each case and the results of pertinent significance tests, which show that the first mode of covariability is robust in each case.

The patterns of covariability produced by MCA are depicted via regressing SST change (homogeneous; e.g. Fig. 3.4b) and zonal wind change (heterogeneous; Fig. 3.4a) onto the SST expansion coefficient. Regression onto the zonal wind expansion coefficient yields similar structures. Here we focus on the SST expansion coefficient as a potential predictor of zonal wind change. A scatter plot of the SST and zonal wind expansion coefficients is depicted as in Fig. 3.4c, and demonstrates their strong correlation in each case.

3.3.2.1 MCA_Full - 300 hPa zonal wind change and Tropical Pacific SST Change

The first pattern of covariability between tropical Pacific SST change and 300 hPa zonal wind change is shown in Fig. 3.4, with the heterogeneous wind change pattern shown in Fig. 3.4a and the homogeneous SST change pattern shown in Fig. 3.4b. Model 2 (MIROC3.2 hires) has been removed from the analysis for MCA_Full because its SST warming from the 20th century to the 21st century is much larger than all other models and significantly changes the first mode of covariability. Model 2 is an outlier for this case only and therefore is included in all other analyses.

The homogeneous SST change field (Fig. 3.4b) shows warming SSTs throughout the entire tropical Pacific basin. Enhanced warming in the eastern equatorial Pacific is reminiscent of the

positive phase of ENSO and spatially correlated with the zonal wind variations associated with temporal ENSO variability in the observed record (Fig. 2.9b, "observed ENSO") at r = 0.47. The heterogeneous wind change pattern (Fig. 3.4a) shows a structure of change that is similar to the ensemble mean wind speed change shown in Fig. 3.2a, including a poleward expansion and weakening of the Pacific jet and a meridional expansion of the Atlantic jet. The heterogeneous wind change pattern exhibits a high spatial correlation with the ensemble mean wind speed change (r = 0.70) but less so with the standard deviation of wind speed change (r = 0.52). The absolute value of the heterogeneous wind change pattern is used in the spatial correlation with the standard deviation of zonal wind change because of the absolute magnitude of variance that is used to calculate the standard deviation. In order to gain further insight into the inter-model variation of the change in winds, modeled ENSO-like tropical Pacific mean state changes are separated from the warming SST change and MCA is repeated.

3.3.2.2 MCA_noGW - 300 hPa zonal wind change and Tropical Pacific SST Change (mean SST change removed)

To remove the global warming signal from the tropical Pacific SST change, the domain-averaged SST change is removed from the raw SST change field in each model prior to performing MCA_noGW (where noGW indicates that the global warming signal has been removed). The resulting pattern of covariability, shown in Fig. 3.5, represents the pattern of zonal wind change that is not associated with domain-averaged warming SSTs.

In this case, the homogeneous SST change pattern (Fig. 3.5b) strongly resembles a positive ENSO pattern and is highly correlated with the observed mean winter ENSO SST pattern (r =

0.77). The heterogeneous wind change pattern (Fig. 3.5a) less strongly resembles the ensemble mean zonal wind change (r = 0.42) and is characterized by increased wind speeds in the Pacific jet exit region. A southward shift of the Atlantic jet near the jet entrance and exit regions is also present. The (absolute value of the) heterogeneous wind change pattern is more highly spatially correlated with the model standard deviation of zonal wind change than in MCA_Full, with r = 0.78, suggesting that changes in model SSTs similar to ENSO-like structures of tropical Pacific SST change are partially responsible for inter-model variations in the portrayal of mid-latitude zonal wind change.

3.3.2.3 MCA_noENSO - 300 hPa zonal wind change and Tropical Pacific SST Change (Winter Mean ENSO (MCA_noGW) removed)

Next, the ENSO-like change signal in the mean winter tropical SSTs is removed from the SST field in order to examine the effects of warming SSTs on mid-latitude zonal wind speed changes in the models. The MCA_noGW heterogeneous zonal wind change pattern is removed from each model's raw wind field, weighted by the standardized wind expansion coefficient for each model. MCA_noGW is used to represent the mean winter ENSO-like SST change pattern because it is highly spatially correlated with the observed mean winter ENSO signal. The same method is used for SST: the homogeneous SST change pattern weighted by each model's standardized SST expansion coefficient is removed from each model's raw SST change field. This process is intended to remove the mean winter ENSO-like signal in each model, weighting the amount of pattern removed by the relative magnitude of the ENSO-like mean SST change pattern in each model. The results of this analysis are shown in Fig. 3.6.

The homogeneous SST change pattern (Fig. 3.6b) shows warming everywhere in the tropical Pacific and is not correlated with the observed ENSO pattern (r = 0.05). The heterogeneous zonal wind change pattern (Fig. 3.6a) resembles the heterogeneous wind change field of MCA_Full and is correlated with the ensemble mean zonal wind change at r = 0.70. The heterogeneous zonal wind change pattern (Fig. 3.6a) shows a northward expansion and weakening of the Pacific jet and a less pronounced northward expansion and weakening of the Atlantic jet. Therefore, the relative warming of mean winter SSTs in each model is related to the northward expansion and weakening of the modeled NH jets.

In order to clarify and emphasize the results from the previous three analyses, Fig. 3.7 summarizes the main findings from MCA of the upper-level zonal wind and SST changes across models. A summary of the spatial correlation between the panels of Fig. 3.7 is found in Table 3.2. Fig. 3.7b shows the heterogeneous zonal wind change field of the mean winter SST change with the ENSO-like change signal removed (MCA_noENSO, Fig. 3.6a). This wind field is spatially correlated with the ensemble mean zonal wind change (Fig. 3.7a) at r = 0.70, signifying that the zonal wind change related to global warming SSTs strongly resembles the ensemble mean zonal wind change. This warming zonal wind change (Fig. 3.7b) is spatially correlated with $-\frac{du}{dy}$ (Fig. 3.7c, a poleward shift of the jet) at r = 0.30, while the ensemble mean zonal wind change is spatially correlated with $-\frac{du}{dy}$ at r = 0.17. Therefore, removing the ENSO-like change signal of MCA_noGW presents a signal that more strongly resembles a poleward shift of the jet, even if it still is not highly correlated with a poleward shift pattern.

Figure 3.7e shows the heterogeneous zonal wind change pattern of the mean winter SST change with the domain-averaged SST change removed (MCA_noGW, Fig. 3.5a). As mentioned above, the absolute value of this pattern is spatially correlated with the model standard deviation (Fig. 3.2b) at r = 0.78, indicating that the ENSO-like change signal is strongly related to inter-model variations in jet stream portrayal. The combination of these analyses suggests that the mean winter ENSO-like change signal of SST variations across models may be masking the theorized poleward shift of the jet in the ensemble mean. This point will be discussed further in Section 3.4.

3.3.2.4 A Comparison at 700 hPa

MCA is repeated for the tropical Pacific SST change and 700 hPa zonal wind change. Fig. 3.8 summarizes the results of a parallel 3-part analysis at 700 hPa (details in Tables 3.1 and 3.2). Overall the results of MCA using the 700 hPa change in zonal wind are very similar to the analysis at 300 hPa. Fig. 3.8b shows the heterogeneous zonal wind field of the mean winter SST change with the ENSO-like signal removed (MCA_noENSO_700). The heterogeneous zonal wind change pattern is correlated with the ensemble mean zonal wind change (Fig. 3.8a) at r = 0.78. In this case the zonal wind change related to warming SSTs resembles the ensemble mean zonal wind change even more strongly than at 300 hPa. This warming zonal wind change is correlated with $-\frac{du}{dy}$ (Fig. 3.8c, a poleward shift of the jet) at r = 0.28, while the ensemble mean zonal wind change is correlated with $-\frac{du}{dy}$ at r = 0.48. Therefore, removing the ENSO-like signal of MCA_noGW_700 presents a signal in this case that less strongly resembles a poleward shift of the jet.

Figure 3.8e shows the heterogeneous zonal wind change pattern of the mean winter SST change with the domain-averaged SST change removed (MCA_noGW_700). The absolute value of this

pattern is spatially correlated with the 700 hPa model standard deviation (not shown) at r = 0.79, again suggesting that the ENSO-like change signal is strongly related to model variations in jet stream changes from the 20th century to the 21st century.

3.3.3 Relationship between Wind Speed Changes and Tropical Pacific SSTs (Regression Analysis)

Using MCA, the ENSO-like SST change signal and warming SST signal have been separated statistically (Section 3.3.2). To verify the results of MCA, an independent investigation is performed using regression analysis. First, the domain-averaged SST change from the 20th century to the 21st century is calculated for the global tropical ocean (27.5°S - 27.5°N, 0° - 360°) for each model. The winter mean cold tongue index (CTI) is also calculated in each model (Zhang et al., 1997). The CTI is a metric that represents the phase of ENSO activity, defined by the SST anomaly pattern over the eastern equatorial Pacific (6°S - 6°N, 180° - 90°W). In this analysis, the CTI change from the 20th century to the 21st century is examined with the domain-averaged SST change removed.

The mean SST change is regressed onto the zonal wind change in each model and the resulting pattern, shown in Fig. 3.9a, resembles both the ensemble mean zonal wind change (shown in red) and the heterogeneous zonal wind change pattern from MCA_noENSO (Fig. 3.6a). The regression field is correlated those patterns at r = 0.80 and r = 0.95 respectively and shows a weakening and northward expansion of the Pacific jet, increased wind speeds in the eastern Pacific, and a slight expansion of the Atlantic jet. This pattern is not highly spatially correlated with the model standard deviation (Fig. 3.2b, r = 0.57). Thus, the modeled warming of SSTs is again shown to be related

to the poleward expansion and weakening of the Pacific jet, and a slight expansion of the Atlantic jet.

When the CTI change (with the domain-averaged SST change removed) is regressed onto the zonal wind change in each model (Fig. 3.9b), the positive wind speed anomaly in the vicinity of the jet exit region strongly resembles the model standard deviation of wind speed change, and the two fields are highly correlated (r = 0.78). This result agrees with the assertion from MCA_noENSO that changes in mean winter SSTs resembling ENSO-like tropical Pacific SSTs are partially responsible for the variation among models in jet stream portrayal, especially in the Pacific.

3.3.4 Inter-Model Variance

To quantify how much the modeled ENSO-like pattern of winter SST change explains variations in jet portrayal among models, Fig. 3.10 examines the inter-model variance of zonal wind changes from the 20th to the 21st century. The inter-model variance is highest in the central Pacific, with a secondary region of variance found in the north Atlantic (Fig. 3.10a). Using the SST expansion coefficients from MCA_noGW and MCA_noENSO as predictors of inter-model variance, the amount of variance explained by each of these patterns can be calculated using regression analysis and are shown in Figs. 3.10b and3.10c for MCA_noGW and the linear combination of MCA_noGW and MCA_noENSO

While 8% of inter-model variance is explained by warming SSTs (not shown), 26% is explained by the ENSO-like signal in each model (Figs. 3.10b). In the central subtropical Pacific region where inter-model variance is maximized, nearly all of the variance is explained by inter-model variations in the ENSO-like pattern of mean winter SST changes. Based upon this result it seems

that if the mean winter change in ENSO from the 20th to the 21st century was more robust in GCMs it would be possible to significantly improve NH jet stream characterization, especially in the Pacific region.

3.4 Conclusions

This study has analyzed changes in NH zonal winds from the 20th century to the 21st century from a non-zonal mean perspective. The ensemble mean zonal wind change at 300 hPa shows a weakening and poleward expansion of the Pacific jet and an overall expansion of the Atlantic jet. These structures are distinct from the theorized poleward shift of the jet and do not consistently project onto internal modes of variability as predicted by the fluctuation-dissipation theory (FDT) at 300 hPa or 700 hPa.

It is important to note that models project varying changes in zonal winds at different levels of the atmosphere. While expansion and weakening are projected of winds in the upper-troposphere, the ensemble mean shows a poleward shift of winds in the lower-troposphere (with relatively large standard deviation). The dissimilarity between levels suggests that the distinct influences of the subtropical and polar jet should be an area of research focus in order to characterize the response of each jet to anthropogenic climate change. It is also interesting to note that in contrast with the direct climate change signal of increasing mid-latitude upper-level winds (e.g. Fig. 3.1), 300 hPa zonal winds are projected to decrease in the core of both the Pacific and Atlantic jets. Increasing 300 hPa zonal winds are located primarily in the jet exit regions as well as on the meridional flanks of the jets.

A statistical examination of the link between mean winter SST changes and zonal wind changes shows that tropical SST differences between models impact the model portrayal of NH jet stream changes. In particular, ENSO-like mean winter SST changes from the 20th century to the 21st century explain 26% of inter-model variation compared to the 8% explained by the domain-averaged warming SST signal identified by MCA and confirmed through regression analysis. This suggests that refining the sign of ENSO changes and its mid-latitude teleconnection patterns in GCMs will increase confidence in the use of models to understand mid-latitude jet stream features under anthropogenic climate change.

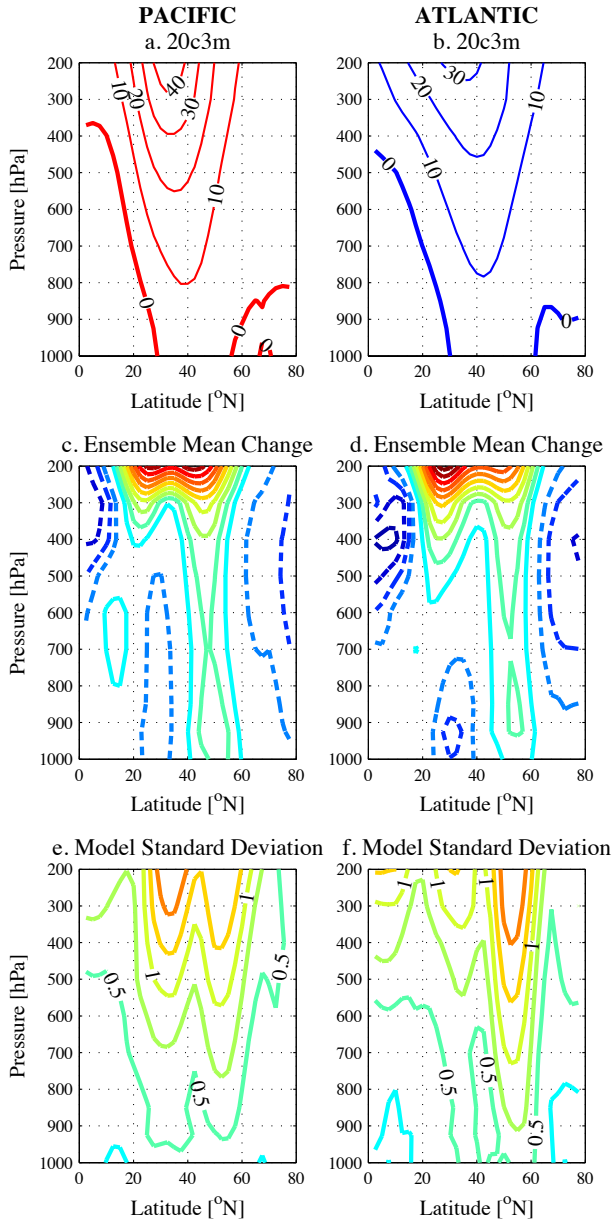

Figure 3.1 Pressure [hPa] vs. Latitude [°N] cross-section showing modeled zonal mean zonal wind. The left column is averaged over 100°E–300°E for the Pacific region and the right column is averaged over 240°E–360° for the Atlantic region. (a)-(b) Ensemble mean 20th century zonal mean zonal wind, contoured every 10 m s^{-1}, (c)-(d) Ensemble mean change of the zonal mean zonal wind, contoured every 0.25 m s^{-1} with negatives dashed and the zero line removed, (e)-(f) Standard deviation of model change of the zonal mean zonal wind about the ensemble mean, contoured every 0.25 m s^{-1}.

a. Ensemble Mean Change in Zonal Wind

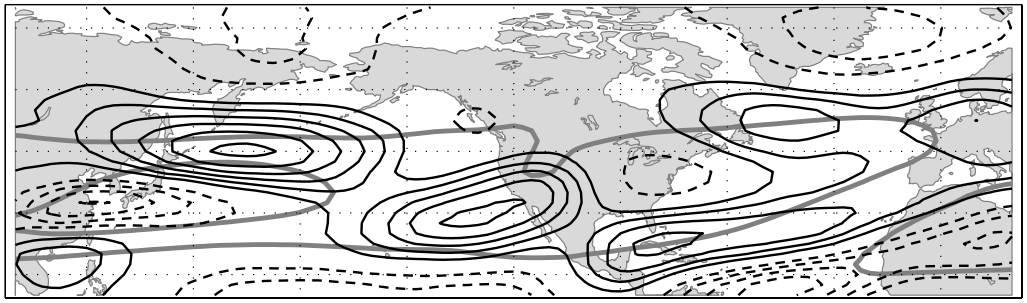

b. Model Standard Deviation of Change in Zonal Wind

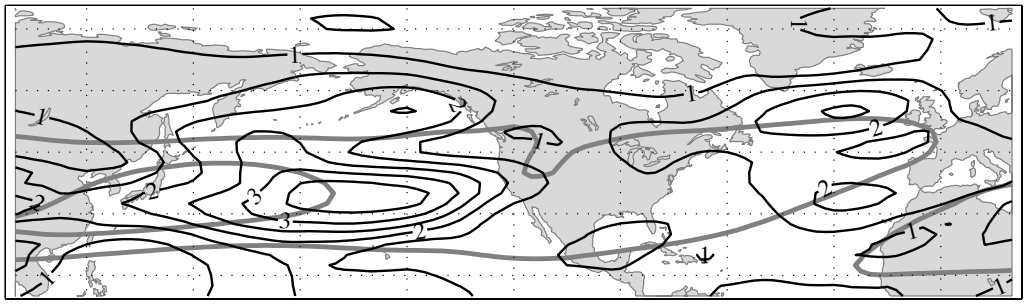

Figure 3.2 (a) Ensemble mean change of the 300 hPa zonal wind from the 20th century to the 21st century, with solid (dashed) lines indicating positive (negative) isotachs, contoured every 0.5 m s^{-1} with the zero line removed. (b) Standard deviation of model change in zonal wind about the ensemble mean for the 17 GCMs under consideration, contoured every 0.5 m s^{-1}. The gray contours show the 20, 40 m s^{-1} isotachs of the ensemble mean winter 300 hPa zonal wind for the 20th century.

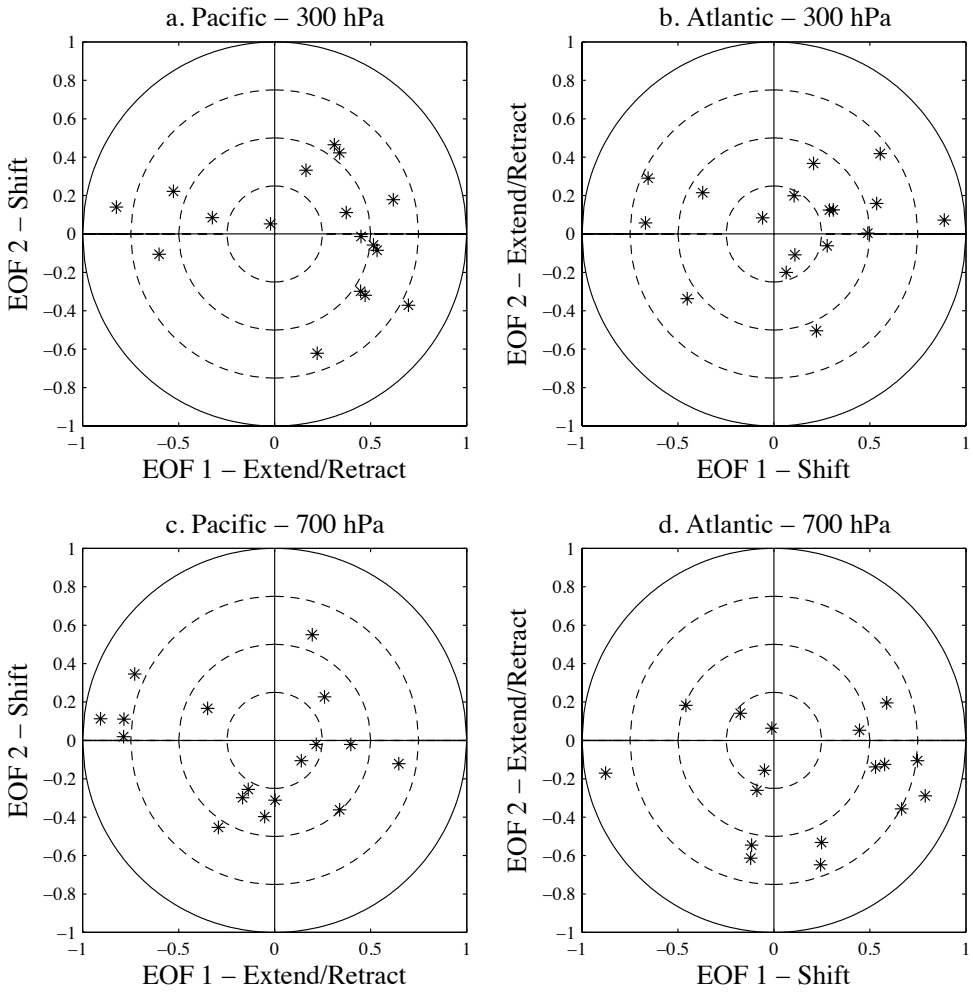

Figure 3.3 Normalized projection of the model change in zonal wind from the 20th century to the 21st century onto EOF 1 and EOF 2 of the 20th century zonal wind from the same model for the (a) 300 hPa Pacific basin, (b) 300 hPa Atlantic basin, (c) 700 hPa Pacific basin, and (d) 700 hPa Atlantic basin. Dashed circles indicate lines of constant projection at 0.25, 0.5, and 0.75.

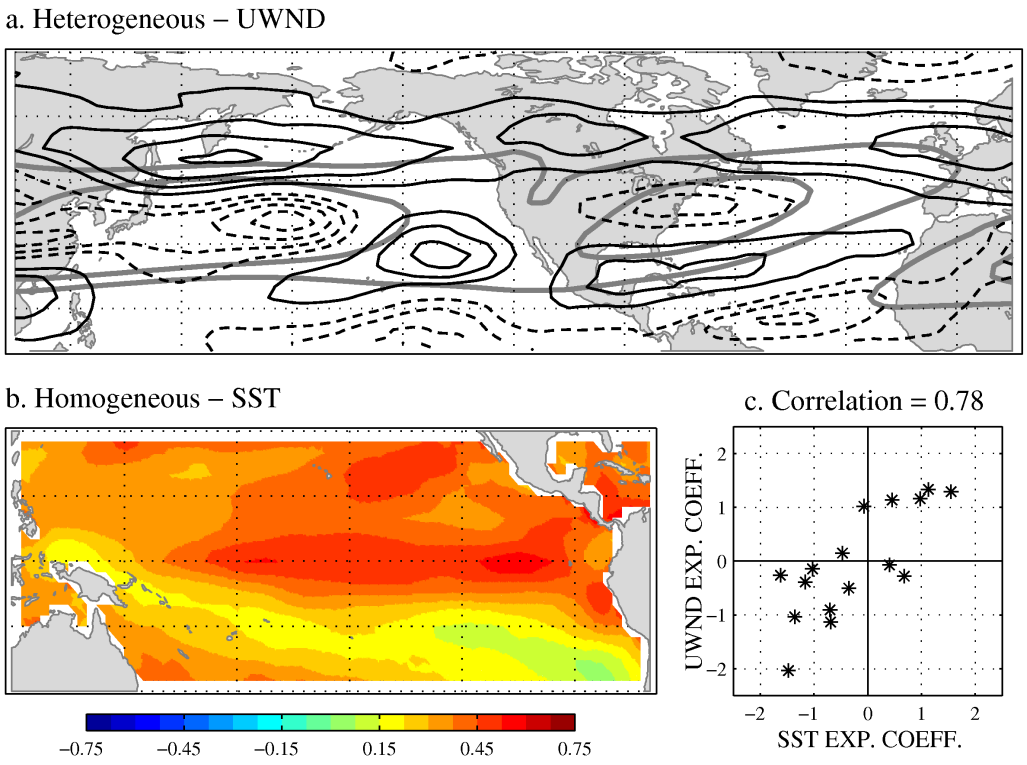

Figure 3.4 Results of MCA of tropical Pacific SST change and mid-latitude 300 hPa zonal wind change from the 20th century to the 21st century (with Model 2 removed). (a) Heterogeneous zonal wind change regression map, (b) Homogeneous SST change regression map, (c) Scatter plot of the wind and SST expansion coefficients. Black solid (dashed) contours in (a) represent positive (negative) perturbation isotachs in units of 0.25 m s^{-1} (with the zero line removed) and gray contours in (a) show the 20, 30 m s^{-1} isotachs of the ensemble mean 300 hPa zonal wind for the 20th century.

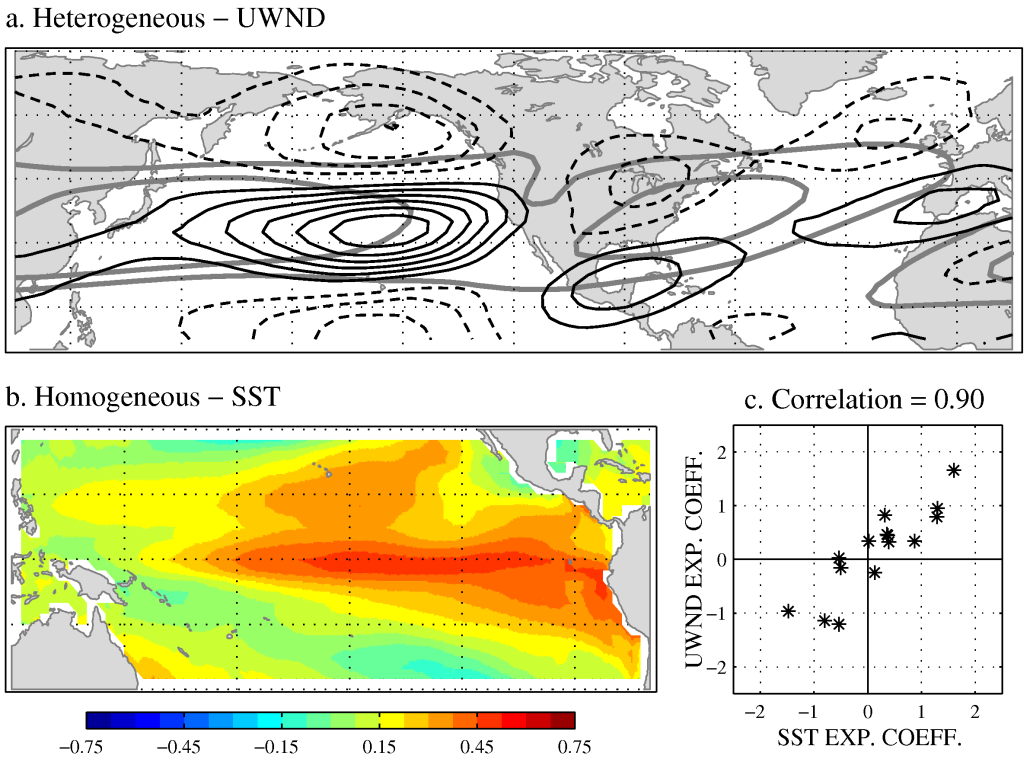

Figure 3.5 Results of MCA of tropical Pacific SST change and mid-latitude 300 hPa zonal wind change (with domain-averaged SST change removed). (a) Heterogeneous zonal wind change regression map, (b) Homogeneous SST change regression map, (c) Scatter plot of the wind and SST expansion coefficients. Black solid (dashed) contours in (a) represent positive (negative) perturbation isotachs in units of 0.5 m s^{-1} (with the zero line removed) and gray contours in (a) show the 20, 30 m s^{-1} isotachs of the ensemble mean 300 hPa zonal wind for the 20th century.

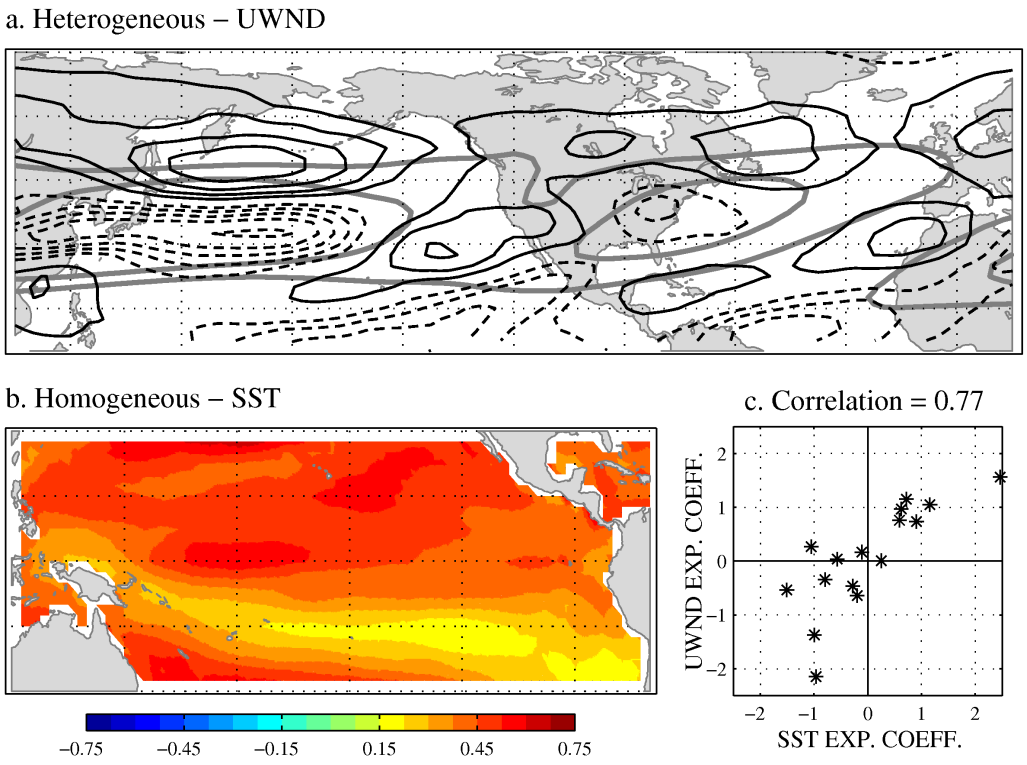

Figure 3.6 Results of MCA of tropical Pacific SST change and mid-latitude 300 hPa zonal wind change (with ENSO-like signal removed, as described in the text). (a) Heterogeneous zonal wind change regression map, (b) Homogeneous SST change regression map, (c) Scatter plot of the wind and SST expansion coefficients. Black solid (dashed) contours in (a) represent positive (negative) perturbation isotachs in units of 0.25 m s^{-1} (with the zero line removed) and gray contours in (a) show the 20, 30 m s^{-1} isotachs of the ensemble mean 300 hPa zonal wind for the 20th century.

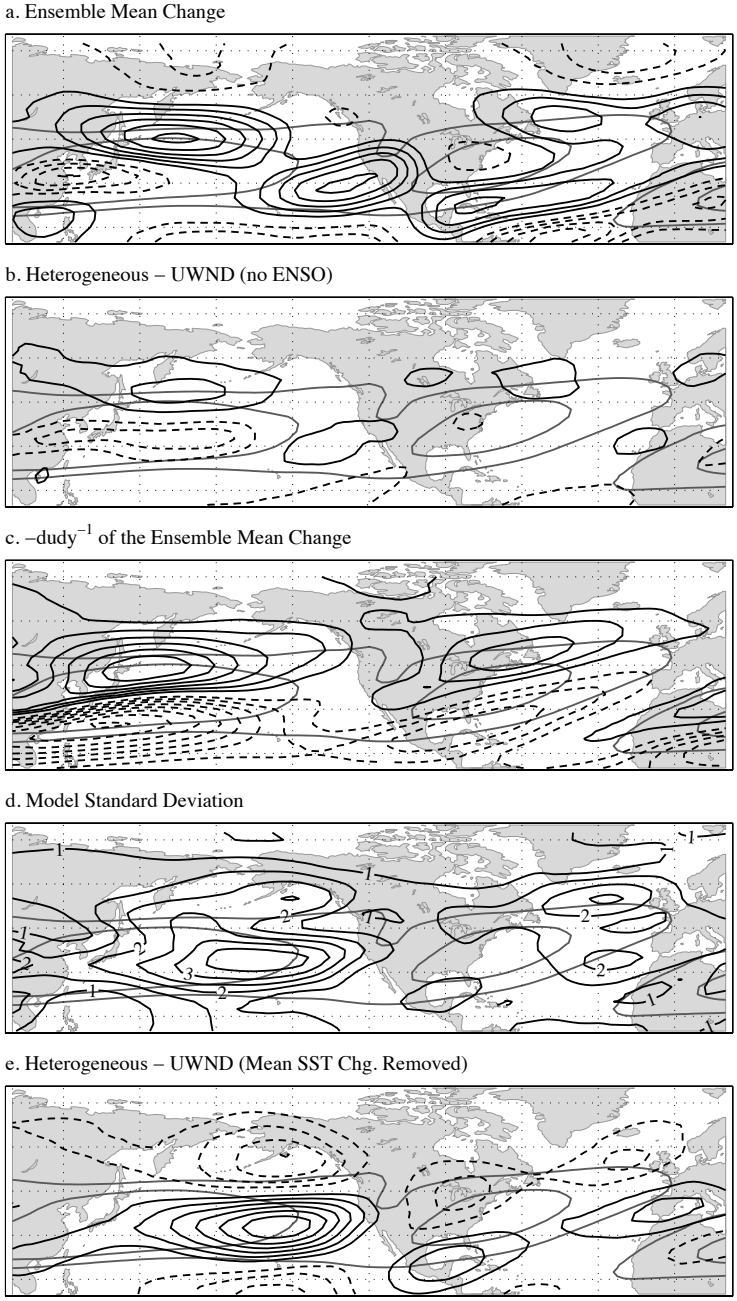

Figure 3.7 (a) Ensemble mean change of the zonal wind, (b) heterogeneous zonal wind change regression map (ENSO-like signal removed, as in 3.6a), (c) $-\frac{du}{dy}$ of the ensemble mean 20th century zonal wind, (d) standard deviation of the change in zonal winds about the ensemble mean, and (d) heterogeneous zonal wind change regression map (with domain-averaged SST change removed, as in 3.5a), all at 300 hPa. The gray lines show the 20, 30 m s^{-1} contours of the ensemble mean 20th century wind at 300 hPa. All panels are contoured every 0.5 m s^{-1} (s^{-1} for (c)) with negative contours dashed and the zero line removed.

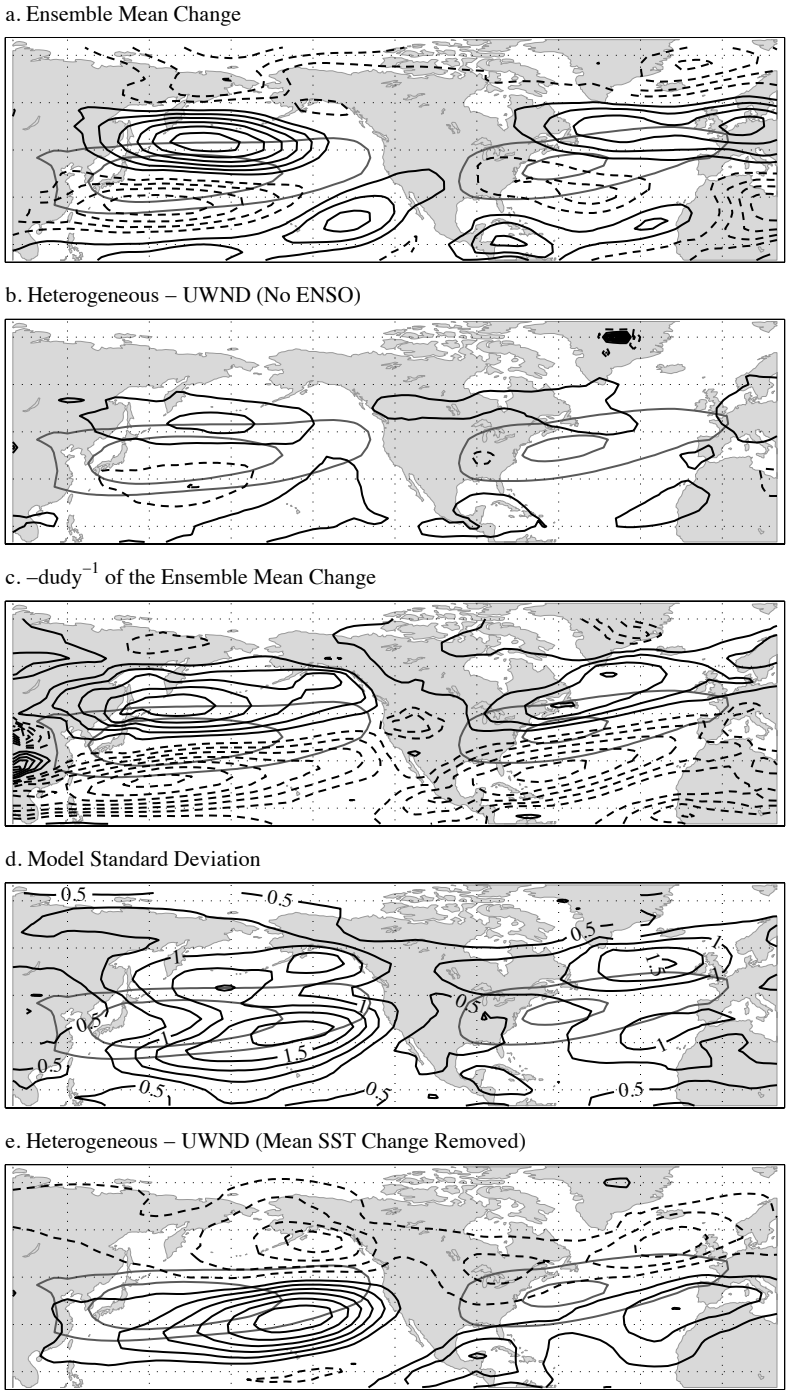

Figure 3.8 (a) Ensemble mean change of the zonal wind, (b) heterogeneous zonal wind change regression map (ENSO-like signal removed), (c) $-\frac{du}{dy}$ of the ensemble mean 20th century zonal wind, (d) standard deviation of the change in zonal winds about the ensemble mean, and (d) heterogeneous zonal wind change regression map (with domain-averaged SST change removed), all at 700 hPa. The gray lines show the 10, 15, 20 m s^{-1} contours of the ensemble mean 20th century winds at 700 hPa. All panels are contoured every 0.25 m s^{-1} (s^{-1} for (c)) with negative contours dashed and the zero line removed.

a. SST Change regressed onto 300 hPa Zonal Wind Change

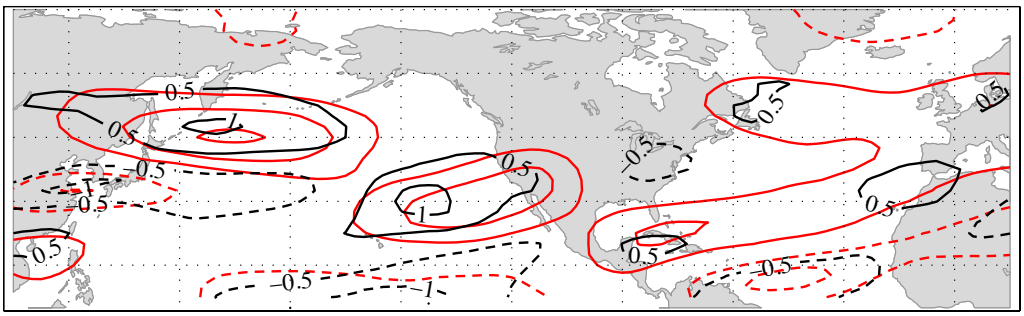

b. CTI (Mean SST Change Removed) regressed onto 300 hPa Zonal Wind Change

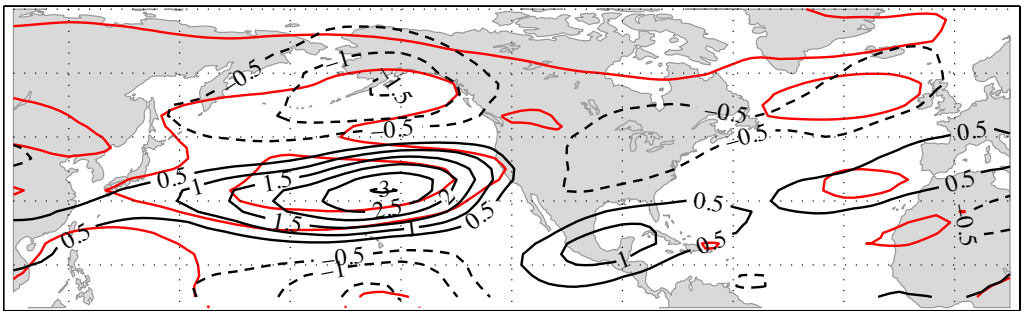

Figure 3.9 (a) Global tropical SST change for each model regressed onto the modeled change in 300 hPa zonal winds and (b) Model CTI (with mean global tropical SST change removed) regressed onto the model change in 300 hPa zonal wind [m s^{-1}]. Black solid (dashed) contours represent positive (negative) perturbation isotachs in units of m s^{-1} (with the zero line removed) and red contours show (a) the ensemble mean change and (b) the standard deviation of the change of the zonal wind change from the 20th century to the 21st century, contoured every 1 m s^{-1}.

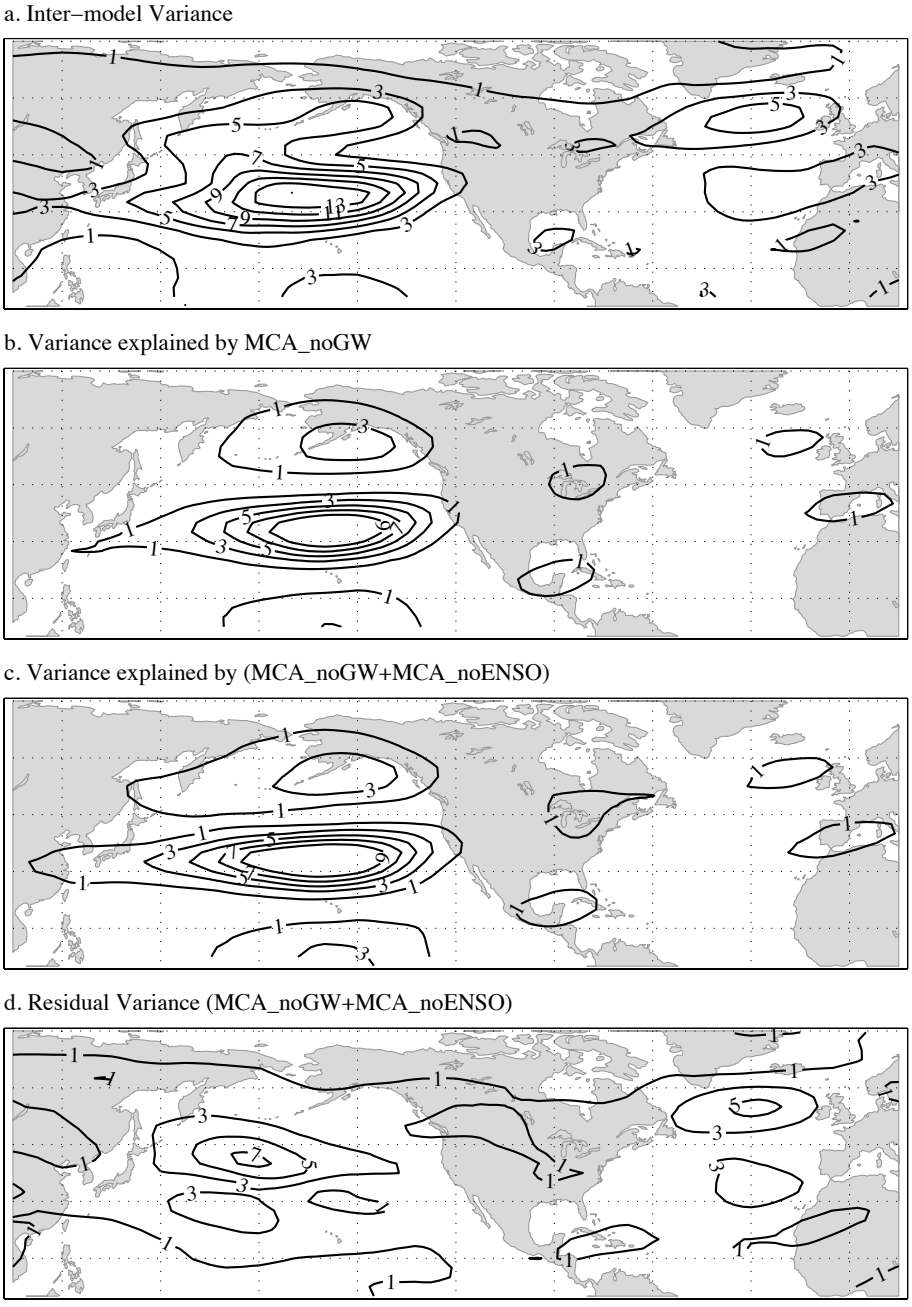

Figure 3.10 (a) Total inter-model variance of the change in the winter 300 hPa zonal wind from the 20th century to the 21st century. Inter-model variance explained by (b) MCA_noGW, (c) Linear combination of MCA_noGW and MCA_noENSO, (d) Residual of MCA_noGW and MCA_noENSO. Variance is contoured every 2 $m^2\ s^{-2}$ starting at 1 $m^2\ s^{-2}$.

Table 3.1 MCA Analysis

MCA	*Description*	*Figure*	*Squared Covariance Fraction* $(1, 2, 3)$	*Normalized Root Mean Squared Covariance*	*Correlation of SST, Wind Expansion Coefficients*
MCA_Full	Tropical Pacific SST Change (Full) and 300 hPa Zonal Wind Change	Fig. 3.4	53%, 28%, 10%	0.28	0.78
MCA_noGW	Tropical Pacific SST Change (Mean SST change removed) and 300 hPa Zonal Wind Change	Fig. 3.5	56%, 17%, 11%	0.31	0.90
MCA_noENSO	Tropical Pacific SST Change (Winter Mean ENSO (MCA2) removed) and 300 hPa Zonal Wind Change	Fig. 3.6	84%, 8%, 3%	0.31	0.77
MCA_Full_700	Tropical Pacific SST Change (Full) and 700 hPa Zonal Wind Change	not shown	62%, 22%, 6%	0.27	0.61
MCA_noGW_700	Tropical Pacific SST Change (Mean SST change removed) and 700 hPa Zonal Wind Change	not shown	55%, 17%, 10%	0.30	0.90
MCA_noENSO_700	Tropical Pacific SST Change (Winter Mean ENSO (MCA5) removed) and 700 hPa Zonal Wind Change	not shown	87%, 5%, 2%	0.31	0.76

Table 3.2 MCA Correlations

$Variable\ 1$	$Variable\ 2$	$Spatial\ Correlation\ (300\ hPa)$	$Spatial\ Correlation\ (700\ hPa)$
Ensemble Mean Change	Heterogeneous UWND (no ENSO)	0.70	0.78
Ensemble Mean Change	$\frac{du}{dy}$	0.17	0.48
Heterogeneous UWND (no ENSO)	$\frac{du}{dy}$	0.30	0.28
Model Standard Deviation	Heterogeneous UWND (no Mean SST Change)	0.39	0.44
Model Standard Deviation	Magnitude of Heterogeneous UWND (no Mean SST Change)	0.78	0.79

Chapter 4

Conclusions

4.1 Summary

Because the portrayal of jet stream winds in CMIP3 GCMs lacks consensus with regard to modeled 20th century and 21st century jet stream structure, the present study focuses on diagnosing inter-model variability of jet portrayal in 17 climate models. It is hoped that knowledge of the factors underlying inter-model variability will contribute to an improvement in the understanding of jet stream changes due to anthropogenic climate change.

The results of the study suggest that targeted improvement of modeled tropical SSTs will significantly improve the modeled extratropical circulation, of which the jet stream is a primary feature. In particular, improved agreement on the sign of projected ENSO changes will improve the portrayal of future jet stream structure. This is an important step toward assessing the impacts of climate change at a variety of scales.

The investigation of ensemble mean biases of 20th century 300 hPa zonal wind suggests that the modeled Atlantic jet is too zonally extended and located too far equatorward compared to the reanalysis. The ensemble mean Pacific jet has less bias than the Atlantic jet, but only because model agreement is much lower and biases in individual models cancel in the ensemble mean.

Mean winter biases in both basins are significant compared to the observed variability of the upper-level zonal winds.

Twenty-first century projections of the ensemble mean zonal wind change at 300 hPa show a weakening and poleward expansion of the Pacific jet and an overall expansion of the Atlantic jet. These structures are distinct from the theorized poleward shift of the jet and do not consistently project onto internal modes of variability as predicted by the fluctuation-dissipation theory (FDT) at 300 hPa or 700 hPa. While expansion and weakening are projected of winds in the upper-troposphere, the ensemble mean shows a poleward shift of winds in the lower-troposphere (with relatively large standard deviation). In contrast with the direct climate change signal of increasing mid-latitude upper-level winds, 300 hPa zonal winds are projected to decrease in the core of both the Pacific and Atlantic jets whereas increasing 300 hPa zonal winds are located primarily in the jet exit regions as well as on the meridional flanks of the jets.

Maximum covariance analysis (MCA) and regression analysis show that the 20th century NH biases in upper-level winds are strongly related to an ENSO-like pattern in winter mean tropical Pacific SSTs. While the present study does not resolve the issue of causality, the similarity between the spatial structure of ENSO's teleconnection in the observed record to the model bias suggests that biases in the tropical Pacific are influencing mid-latitude zonal wind biases. Examination of the link between mean winter SST changes and zonal wind changes from the 20th century and the 21st century shows that SST change differences between models impact the model portrayal of NH jet stream changes. In particular, ENSO-like mean winter SST changes explain 26% of inter-model variation compared to the 8% explained by the domain-averaged warming SST signal.

Temporal variability of the upper-level zonal winds in the 20th century is accurately modeled in nearly all 17 GCMs. Furthermore, it is shown that in the Pacific, model biases that exist in the portrayal of EOF 1 and EOF 2 are strongly linked to the modeled longitude of the jet exit in the Pacific region. This result implies that an improved characterization of the mean state of the Pacific jet will also positively impact the modeled variability.

In conclusion, results herein indicate that improvements in model portrayal of 20th century tropical Pacific winter SSTs will significantly advance the portrayal of the modeled 20th century winter Pacific and Atlantic jets, and will consequently improve the modeled jet stream variability in the Pacific. In addition, the refinement of the sign of future ENSO changes will increase consistency in modeled mid-latitude jet stream features under anthropogenic climate change.

The broad similarity between the ensemble mean zonal wind changes and the zonal wind changes predicted by warming SSTs is promising. Even though varying model portrayals of the change of the mean winter ENSO-like tropical Pacific SSTs strongly affect zonal wind changes, models are spread evenly around the ensemble mean. It is important to know that the sign of future ENSO change and the overall future tropical SST warming are the two dominant predictors of zonal wind changes in GCMs. An improvement of the consistency and accuracy of ENSO portrayal is most important and will unmask previously unknown characteristics of the climate change signal in NH zonal winds.

4.2 Avenues of Future Research

The use of a non-zonally averaged approach for the examination of jet stream structure in climate models is applicable far beyond the reaches of this single study. To complete a global inspection of the portrayal of the jet in climate models, it would be necessary to include the Southern Hemisphere eddy-jet system, as well as other seasons of the year. In addition, a comparison study with other SRES scenarios in the CMIP3 dataset would make it possible to compare the signal generated from different levels of climate change, creating a range of possible outcomes of jet structure as well as a range of model differences that might lend further insight into the dynamics underlying variations in jet structure. Also, improved models for the earth system are constantly being presented, and it is necessary to find a good balance between adequate analysis of the strengths and weaknesses of each model and adaptation to newer, more powerful modeling tools that are available. To that end, it is important that this study be reproduced on the CMIP5 dataset, which is newly available. It is possible that many of the biases identified in this study have already been corrected in the new suite of models.

One example of jet variability that could easily be studied in conjunction with the present study is the midwinter suppression of the Pacific storm track, originally defined by Nakamura (1992), referring to the unexpected minimum of storm track activity during mid-winter months despite a maximum in baroclinicity over the Pacific basin. Defining storm track activity based upon the average eddy kinetic energy of November, January, and 15 March - 15 April, following Nakamura (1992), the midwinter suppression was examined in the 17 GCMs considered in the present study. Twelve of the seventeen GCMs do include a feature resembling the midwinter suppression of

the 20th century Pacific storm track. However, the magnitude of the midwinter suppression is not found to be related to the intensity of the jet stream in the models, suggesting that other mechanisms may be responsible for producing this feature within GCMs. Further investigation of this topic will certainly lend insight into the dynamics of the eddy-jet system in the Northern Hemisphere Pacific.

MCA has been shown to be an advantageous tool for assessing co-varying parameters across multiple GCMs. While MCA is often used to understand variables that co-vary temporally, this new application of MCA is a powerful way to determine inter-model reliability. While the jet is an important and primary variable of the atmospheric large-scale circulation, there are other variables that deviate widely among models for which this type of analysis would be quite beneficial. MCA has been used as the basis for downscaling studies in the past and could also provide a useful counterpart to GCM downscaling studies used to examine regional-scale climate model projections. For example, MCA could be used to investigate the covariability between tropical Pacific SST biases and North American precipitation biases simulated by models.

This study has been completed primarily with the use of a *climate* paradigm approach. The investigations detailed here began with winter-averaged data that was used to identify the jet stream and then classify jet variability through the use of EOF/PC analysis. It would be very interesting to complete a similar study using a *weather* paradigm approach, identifying a certain type of jet structure in daily climate model data and then scaling up to examine the winter season as a compilation of these events. For instance, jet retraction events (Jaffe et al., 2011) could be identified in the daily data for each winter in each of the climate models used in this study. A model inter-comparison

could identify differences in frequency of jet retractions among models as well as compared to observations.

On a similar note, the present study has suggested that there are significant differences between jet structures at different levels of the atmosphere, likely related to the varying influences of the subtropical and polar jets in different regions of the globe at different altitudes. Currently, an interesting study is underway that seeks to separate the influences of these two jet structures every 6 hours in multiple reanalysis datasets (J.E. Martin, personal communication). Expanding this project to include climate model data and compiling the influences of the subtropical and polar jets over the course of an average winter season would be very complementary to the *climate* paradigm research presented in this study. A functional partnership between these two perspectives will make huge strides in understanding the mechanisms responsible for jet stream structure changes under anthropogenic climate change.

Bibliography

Bengtsson, L., K. Hodges, and E. Roeckner, 2006: Storm tracks and climate change. *Journal of Climate*, **19 (15)**, 3518–3543.

Blackmon, M., 1976: A climatological spectral study of the 500 mb geopotential height of the northern hemisphere. *Journal of Atmospheric Sciences*, **33**, 1607–1623.

Blackmon, M., Y. Lee, J. Wallace, and H. Hsu, 1984: Time variation of 500 mb height fluctuations with long, intermediate and short time scales as deduced from lag-correlation statistics(in synoptic atmospheric circulation). *Journal of the atmospheric sciences*, **41**, 981–991.

Blackmon, M., J. Wallace, N. Lau, and S. Mullen, 1977: An observational study of the northern hemisphere wintertime circulation. *Journal of Atmospheric Sciences*, **34**, 1040–1053.

Bretherton, C., C. Smith, J. Wallace, et al., 1992: An intercomparison of methods for finding coupled patterns in climate data. *Journal of climate*, **5 (6)**, 541–560.

Bryson, R., 1994: The discovery of the jet stream. *Wisconsin Acadmy Review*, 15–17.

Chang, E., 1993: Downstream development of baroclinic waves as inferred from regression analysis. *Journal of the atmospheric sciences*, **50 (13)**, 2038–2053.

Chang, E., S. Lee, and K. Swanson, 2002: Storm track dynamics. *Journal of climate*, **15 (16)**, 2163–2183.

Charney, J., 1947: The dynamics of long waves in a baroclinic westerly current. *J. Meteor*, **4 (5)**, 135–162.

Chen, G. and I. Held, 2007: Phase speed spectra and the recent poleward shift of southern hemisphere surface westerlies. *Geophys. Res. Lett*, **34**, L21 805.

Chen, G., I. Held, and W. Robinson, 2007: Sensitivity of the latitude of the surface westerlies to surface friction. *Journal of the atmospheric sciences*, **64 (8)**, 2899–2915.

Delworth, T., et al., 2006: Gfdl's cm2 global coupled climate models. part i: Formulation and simulation characteristics. *Journal of Climate*, **19 (5)**, 643–674.

Deser, C. and M. Timlin, 1997: Atmosphere-ocean interaction on weekly timescales in the north atlantic and pacific. *Journal of climate*, **10 (3)**, 393–408.

Donohoe, A. and D. Battisti, 2009: Causes of reduced north atlantic storm activity in a cam3 simulation of the last glacial maximum. *Journal of Climate*, **22 (18)**, 4793–4808.

Eady, E., 1949: Long waves and cyclone waves. *Tellus*, **1 (3)**, 33–52.

Eichelberger, S. and D. Hartmann, 2007: Zonal jet structure and the leading mode of variability. *Journal of Climate*, **20 (20)**, 5149–5163.

Flato, G., G. Boer, W. Lee, N. McFarlane, D. Ramsden, M. Reader, and A. Weaver, 2000: The canadian centre for climate modelling and analysis global coupled model and its climate. *Climate Dynamics*, **16 (6)**, 451–467.

Galin, V. Y., E. M. Volodin, and S. P. Smyshliaev, 2003: Atmosphere general circulation model of inm ras with ozone dynamics. *Russian meteorology and hydrology*, **N (5)**, 13–22.

Gerber, E., L. Polvani, and D. Ancukiewicz, 2008a: Annular mode time scales in the intergovernmental panel on climate change fourth assessment report models. *Geophysical Research Letters*, **35 (22)**, L22 707.

Gerber, E., S. Voronin, and L. Polvani, 2008b: Testing the annular mode autocorrelation time scale in simple atmospheric general circulation models. *Monthly Weather Review*, **136 (4)**, 1523–1536.

Gnanadesikan, A., et al., 2006: Gfdl's cm2 global coupled climate models. part ii: The baseline ocean simulation. *Journal of climate*, **19 (5)**, 675–697.

Gordon, H. et al., 2002: The csiro mk3 climate system model. Tech. rep., CSIRO.

Gualdi, S., E. Scoccimarro, A. Bellucci, A. Grezio, E. Manzini, and A. Navarra, 2006: The main features of the 20th century climate as simulated with the sxg coupled gcm. *Claris Newsletter*, **none (4)**.

Gualdi, S., E. Scoccimarro, A. Navarra, et al., 2008: Changes in tropical cyclone activity due to global warming: Results from a high-resolution coupled general circulation model. *Journal of climate*, **21 (20)**, 5204–5228.

Hasumi, H. and S. Emori, 2004: K-1 coupled gcm (miroc) description. *Center for Climate System Research, University of Tokyo, National Institute for Environmental Studies, Frontier Research Center for Global Change, Tokyo, Japan*, **38**.

Held, I., 1993: Large-scale dynamics and global warming. *Bulletin of the American Meteorological Society*, **74 (2)**, 228–242.

Hoskins, B., I. James, and G. White, 1983: The shape, propagation and mean-flow interaction of large-scale weather systems. *Journal of the atmospheric sciences*, **40 (7)**, 1595–1612.

Hoskins, B. and D. Karoly, 1981: The steady linear response of a spherical atmosphere to thermal and orographic forcing. *Journal of the Atmospheric Sciences*, **38 (6)**, 1179–1196.

Hoskins, B. and P. Valdes, 1990: On the existence of storm-tracks. *Journal of the atmospheric sciences*, **47**, 1854–1864.

Hu, Y., Q. Fu, et al., 2007: Observed poleward expansion of the hadley circulation since 1979. *Atmospheric Chemistry and Physics*, **7 (19)**, 5229–5236.

Ihara, C. and Y. Kushnir, 2009: Change of mean midlatitude westerlies in 21st century climate simulations. *Geophysical Research Letters*, **36 (13)**, L13 701.

Jaffe, S., J. Martin, D. Vimont, and D. Lorenz, 2011: A synoptic climatology of episodic, subseasonal retractions of the pacific jet. *Journal of climate*, **24 (11)**, 2846–2860.

Johanson, C. and Q. Fu, 2009: Hadley cell widening: Model simulations versus observations. *Journal of Climate*, **22 (10)**, 2713–2725.

Jungclaus, J., et al., 2006: Ocean circulation and tropical variability in the coupled model echam5/mpi-om. *Journal of Climate*, **19 (16)**, 3952–3972.

Kalnay, E., et al., 1996: The ncep/ncar 40-year reanalysis project. *Bulletin of the American Meteorological Society*, **77 (3)**, 437–471.

Karpechko, A., 2010: Uncertainties in future climate attributable to uncertainties in future northern annular mode trend. *Geophysical Research Letters*, **37 (20)**, L20 702.

Kidston, J., S. Dean, J. Renwick, and G. Vallis, 2010: A robust increase in the eddy length scale in the simulation of future climates. *Geophys. Res. Lett*, **37**, L03 806.

Kidston, J. and E. Gerber, 2010: Intermodel variability of the poleward shift of the austral jet stream in the cmip3 integrations linked to biases in 20th century climatology. *Geophys. Res. Lett*, **37**, L09 708.

Kidston, J., G. Vallis, S. Dean, and J. Renwick, 2011: Can the increase in the eddy length scale under global warming cause the poleward shift of the jet streams? *Journal of Climate*, **24 (14)**, 3764–3780.

Klein, W., 1957: *Principal tracks and mean frequencies of cyclones and anticyclones in the Northern Hemisphere*. US Government Printing Office.

Kushner, P., I. Held, and T. Delworth, 2001: Southern hemisphere atmospheric circulation response to global warming. *J. Clim.*, **14**, 2238–2249.

Lau, N., 1988: Variability of the observed midlatitude storm tracks in relation to low- frequency changes in the circulation pattern. *Journal of the atmospheric sciences*, **45 (19)**, 2718–2743.

Leith, C., 1975: Climate response and fluctuation dissipation. *Journal of the Atmospheric Sciences*, **32 (10)**, 2022–2026.

Lorenz, D. and E. DeWeaver, 2007: Tropopause height and zonal wind response to global warming in the ipcc scenario integrations. *Journal of Geophysical Research*, **112 (D10)**, 10 119.

Lorenz, D. and D. Hartmann, 2003: Eddy-zonal flow feedback in the northern hemisphere winter. *Journal of climate*, **16 (8)**, 1212–1227.

Lu, J., G. Chen, and D. Frierson, 2008: Response of the zonal mean atmospheric circulation to el niño versus global warming. *Journal of Climate*, **21 (22)**, 5835–5851.

Lu, J., G. Chen, and D. Frierson, 2010: The position of the midlatitude storm track and eddy-driven westerlies in aquaplanet agcms. *Journal of the Atmospheric Sciences*, **67 (12)**, 3984–4000.

Lu, J., G. Vecchi, and T. Reichler, 2007: Expansion of the hadley cell under global warming. *Geophys. Res. Lett*, **34 (1.06805)**.

Lucarini, V. and G. Russell, 2002: Comparison of mean climate trends in the northern hemisphere between national centers for environmental prediction and two atmosphere-ocean model forced runs. *J. Geophys. Res*, **107 (10.1029)**.

Manabe, S. and R. Stouffer, 1980: Sensitivity of a global climate model to an increase of co 2 concentration in the atmosphere. *Journal of Geophysical Research*, **85 (C10)**, 5529–54.

Marshall, G., 2003: Trends in the southern annular mode from observations and reanalyses. *Journal of Climate*, **16 (24)**, 4134–4143.

Meehl, G., C. Covey, T. Delworth, M. Latif, B. McAvaney, J. Mitchell, R. Stouffer, and K. Taylor, 2007: The WCRP CMIP3 multi-model dataset: A new era in climate change research. *Bull. Amer. Meteor. Soc.*, **88**, 1383–1394.

Nakamura, H., 1992: Midwinter suppression of baroclinic wave activity in the pacific. *Journal of Atmospheric Sciences*, **49**, 1629–1642.

Nakicenovic, N., 2000: Greenhouse gas emissions scenarios. *Technological Forecasting and Social Change*, **65 (2)**, 149–166.

North, G., T. Bell, R. Cahalan, and F. Moeng, 1982: Sampling errors in the estimation of empirical orthogonal functions. *Mon. Wea. Rev*, **110 (7)**, 699–706.

Orlanski, I., 1998: Poleward deflection of storm tracks. *Journal of the atmospheric sciences*, **55 (16)**, 2577–2602.

Orlanski, I., 2005: A new look at the pacific storm track variability: Sensitivity to tropical ssts and to upstream seeding. *Journal of the atmospheric sciences*, **62 (5)**, 1367–1390.

Orlanski, I. and E. Chang, 1993: Ageostrophic geopotential fluxes in downstream and upstream development of baroclinic waves. *Journal of the atmospheric sciences*, **50 (2)**, 212–225.

Orlanski, I. and J. Sheldon, 1995: Stages in the energetics of baroclinic systems. *Tellus A*, **47 (5)**, 605–628.

Overland, J. and M. Wang, 2005: The arctic climate paradox: The recent decrease of the arctic oscillation. *Geophys. Res. Lett*, **32 (6)**, L06 701.

Petterssen, S., 1956: *Weather Analysis and Forecasting, Vol. 1, 2nd. ed.* McGraw-Hill.

Reiter, E., 1963: *Jet-stream meteorology*. University of Chicago Press.

Reiter, E., 1967: *Jet streams; how do they affect our weather?* Doubleday.

Ring, M. and R. Plumb, 2008: The response of a simplified gcm to axisymmetric forcings: Applicability of the fluctuation-dissipation theorem. *Journal of the Atmospheric Sciences*, **65 (12)**, 3880–3898.

Russell, G., J. Miller, and D. Rind, 1995: A coupled atmosphere-ocean model for transient climate change studies. *Atmosphere-ocean*, **33 (4)**, 683–730.

Sawyer, J., 1970: Observational characteristics of atmospheric fluctuations with a time scale of a month. *Quarterly Journal of the Royal Meteorological Society*, **96 (410)**, 610–625.

Schmidt, G., et al., 2006: Present-day atmospheric simulations using giss modele: Comparison to in situ, satellite, and reanalysis data. *Journal of Climate*, **19 (2)**, 153–192.

Serreze, M., A. Barrett, J. Stroeve, D. Kindig, and M. Holland, 2009: The emergence of surface-based arctic amplification. *The Cryosphere*, **3 (1)**, 11–19.

Simmons, A. and B. Hoskins, 1979: The downstream and upstream development of unstable baroclinic waves. *Journal of Atmospheric Sciences*, **36**, 1239–1254.

Solomon, S., 2007: *Climate change 2007: the physical science basis: contribution of Working Group I to the Fourth Assessment Report of the Intergovernmental Panel on Climate Change*. Cambridge Univ Pr.

Straus, D. and J. Shukla, 2002: Does enso force the pna? *Journal of climate*, **15 (17)**, 2340–2358.

Thompson, D. and J. Wallace, 2000: Annular modes in the extratropical circulation. part i: Month-to-month variability. *Journal of Climate*, **13 (5)**, 1000–1016.

Thompson, D., J. Wallace, and G. Hegerl, 2000: Annular modes in the extratropical circulation. part ii: Trends. *Journal of Climate*, **13 (5)**, 1018–1036.

Trenberth, K., G. Branstator, and D. Karoly, 1998: Progress during toga in understanding and modeling global teleconnections associated with tropical. *Journal of Geophysical Research*, **103**, 14–291.

Ulbrich, U., J. Pinto, H. Kupfer, G. Leckebusch, T. Spangehl, and M. Reyers, 2008: Changing northern hemisphere storm tracks in an ensemble of ipcc climate change simulations. *Journal of Climate*, **21 (8)**, 1669–1679.

Valdes, P. and B. Hoskins, 1989: Linear stationary wave simulations of the time-mean climatological flow. *Journal of Atmospheric Sciences*, **46**, 2509–2527.

Vimont, D., D. Battisti, and A. Hirst, 2001: Footprinting: A seasonal connection between the tropics and mid-latitudes. *Geophys. Res. Lett*, **28 (20)**, 3923–3926.

Volodin, E. and N. Diansky, 2004: El-niño reproduction in a coupled general circulation model of atmosphere and ocean. *Russ. Meteorol. Hydrol*, **12**, 5–14.

Wallace, J., G. Lim, and M. Blackmon, 1988: Relationship between cyclone tracks, anticyclone tracks and baroclinic waveguides. *Journal of the atmospheric sciences*, **45 (3)**, 439–462.

Wallace, J., C. Smith, C. Bretherton, et al., 1992: Singular value decomposition of wintertime sea surface temperature and 500-mb height anomalies. *Journal of climate*, **5 (6)**, 561–576.

Wallace, J. M. and D. S. Gutzler, 1981: Teleconnections in the geopotential height field during the northern hemisphere winter. *Monthly Weather Review*, **109**, 784–812.

Wang, H. and R. Fu, 2000: Winter monthly mean atmospheric anomalies over the north pacific and north america associated with el nino ssts. *Journal of climate*, **13 (19)**, 3435–3447.

Woollings, T., 2008: Vertical structure of anthropogenic zonal-mean atmospheric circulation change. *Geophys. Res. Lett*, **35**, L19 702.

Woollings, T. and M. Blackburn, 2012: The north atlantic jet stream under climate change, and its relation to the nao and ea patterns. *Journal of Climate*, **25 (3)**, 886–902.

Wu, Y., M. Ting, R. Seager, H. Huang, and M. Cane, 2010: Changes in storm tracks and energy transports in a warmer climate simulated by the gfdl cm2. 1 model. *Climate dynamics*, **37 (1)**, 53.

Yaocun, Z. and H. Daqing, 2011: Has the east asian westerly jet experienced a poleward displacement in recent decades? *Advances in Atmos. Sciences*, **28 (6)**, 1259–1265.

Yin, J., 2002: The peculiar behavior of baroclinic waves during the midwinter suppression of the pacific storm track. *Ph.D. thesis, University of Washington*, 121 pp.

Yin, J., 2005: A consistent poleward shift of the storm tracks in simulations of 21st century climate. *Geophysical Research Letters*, **32 (18)**, 2–5.

Yu, Y., R. Yu, X. Zhang, and H. Liu, 2002: A flexible coupled ocean-atmosphere general circulation model. *Advances in Atmospheric Sciences*, **19 (1)**, 169–190.

Yu, Y., X. Zhang, and Y. Guo, 2004: Global coupled ocean-atmosphere general circulation models in lasg/iap. *Advances in Atmospheric sciences*, **21 (3)**, 444–455.

Yukimoto, S., et al., 2006: Present-day climate and climate sensitivity in the meteorological research institute coupled gcm version 2.3 (mri-cgcm2. 3). *Journal of the Meteorological Society of Japan*, **84 (2)**, 333–363.

Zhang, Y., J. Wallace, and D. Battisti, 1997: Enso-like interdecadal variability: 1900-93. *Journal of Climate*, **10 (5)**, 1004–1020.